nature communications

Article

https://doi.org/10.1038/s41467-025-63170-2

Prolonged exposure to food odors suppresses feeding via an olfactory bulb-to-hypothalamus circuit

Received: 27 October 2024

Accepted: 7 August 2025

Published online: 23 August 2025

Check for updates

Yao Liu[1,2,12], Hailan Liu[3,11,12], Huey-Xian Kelly Wong[1,2], Niccole Auld[4,5,6], Kristine M. Conde[3,11], Yongxiang Li[3,11], Meng Yu[3], Yue Deng[3,11], Qingzhuo Liu[3,11], Xing Fang[1,2], Mengjie Wang[3,11], Yuhan Shi[3], Olivia Z. Ginnard[3], Yuxue Yang[3,11], Longlong Tu[3,11], Hesong Liu[3], Jonathan C. Bean[3], Junying Han[3], Megan E. Burt[3], Sanika V. Jossy[3], Yongjie Yang[3,11], Chunmei Wang[3], Qingchun Tong[7], Benjamin R. Arenkiel[1,6,8], Hongjie Li[5,6], Yong Xu[3,9,10,11] ✉ & Yang He[1,2] ✉

Olfactory perception of food odors is a key determinant of eating behavior, including triggering appetite, facilitating food seeking and influencing food choice. While transient food-related olfactory cues stimulate appetite and provoke cravings in states of hunger, emerging evidence implies that prolonged and sustained exposure to food-derived odor (FO) suppresses feeding. However, the mechanisms by which olfaction induces hypophagia remain elusive. In this study, we show that prolonged FO exposure significantly suppresses food intake in male mice. We identified a subset of neurons in the ventral subiculum (vSub) that are specifically activated by FO. We further discovered that these FO-activated neurons in the vSub receive excitatory inputs from the olfactory bulb (OB) and send glutamatergic projections to the ventromedial hypothalamus (VMH). Inhibition of the OB → vSub → VMH circuit abolished the FO-induced reduction in food intake, while activation of this circuit suppressed feeding and reduced body weight. Together, these findings reveal a neurobiological circuitry that mediates the influence of olfactory signals on food intake regulation.

Obesity is a worldwide epidemic, increasing risk of mortality by contributing to serious, debilitating health conditions such as heart disease, stroke, diabetes, and some cancers[1] with an estimated health care cost of more than 425.5 billion dollars in the US in 2023[2]. The role of homeostatic mechanisms in which internal signals such as leptin, ghrelin, and insulin communicate with various brain regions to modulate food intake and energy expenditure—and therefore obesity—have been well described[3–5]. However, the integration of external

[1]Jan and Dan Duncan Neurological Research Institute, Texas Children's Hospital, Houston, TX, USA. [2]Section of Neurology, Department of Pediatrics, Baylor College of Medicine, Houston, TX, USA. [3]Department of Pediatrics, USDA/ARS Children's Nutrition Research Center, Baylor College of Medicine, Houston, TX, USA. [4]Program in Cancer Cell Biology, Baylor College of Medicine, Houston, TX, USA. [5]Huffington Center on Aging, Baylor College of Medicine, Houston, TX, USA. [6]Department of Molecular and Human Genetics, Baylor College of Medicine, Houston, TX, USA. [7]Brown Foundation Institute of Molecular Medicine, University of Texas Health Science Center at Houston, Houston, TX, USA. [8]Department of Neuroscience, Baylor College of Medicine, Houston, TX, USA. [9]Department of Molecular and Cellular Biology, Baylor College of Medicine, Houston, TX, USA. [10]Department of Medicine, Baylor College of Medicine, Houston, TX, USA. [11]Present address: Department of Psychiatry and Behavioral Neuroscience, University of South Florida, Tampa, FL, USA. [12]These authors contributed equally: Yao Liu, Hailan Liu. ✉e-mail: yongx@bcm.edu; yang.he@bcm.edu

signals, such as smell, towards energy homeostasis is increasingly recognized as pivotal for eating behaviors. Olfaction serves as a powerful modulator, influencing appetite, food preferences, and overall eating experience[6–9]. While transient olfaction cues of food can influence appetite and trigger food cravings in a state of hunger[9–11], emerging evidence implies that prolonged food odor exposure suppresses food intake in both humans and animals[12–14]. For example, normal-weight children consumed fewer sweet and savory snacks after being exposed to the smell of these foods for a period of time compared to those not exposed to food-related odors[12]. Similarly, healthy women reported a decreased appetite for chocolate after smelling it[14]. In *Drosophila*, sustained exposure to food-related odors from vinegar or yeast, common foods for these flies, also led to reduced food intake[13]. Interestingly, enhancement of olfactory sensory neuron (OSN) signaling through genetic manipulation to increase the expression of short neuropeptide F (sNPF) leads to a reduction in feeding in *Drosophila*[13]. These findings underscore that augmenting the olfactory pathway, either through reinforced olfactory input or genetic manipulation, suppresses food intake. However, it remains unclear whether the effect is specific to food-related odor and which neural circuits connect olfactory information to feeding circuits. Understanding the mechanisms underlying this phenomenon could lead to new treatments for obesity.

The ventral subiculum (vSub) forms the CA1-entorhinal transition zone of the hippocampal formation[15]. It receives inputs from areas such as the hippocampal CA1, entorhinal cortex, prefrontal cortex, amygdala, and thalamus, and projects to the nucleus accumbens, lateral septum, ventral tegmental area, hypothalamus, prefrontal cortex, and habenula[16,17]. This extensive connectivity with other brain regions governs important and diverse functions of vSub neurons. Indeed, considerable evidence indicates that the vSub regulates a wide range of behaviors, including stress[18–20], memory and spatial navigation[21], reward and motivation[22–24], as well as neuroendocrine functions[19]. Notably, the vSub has been shown to be involved in integrating sensory information and translating it into appropriate behavioral responses. This includes processing auditory, olfactory, and visual cues that are crucial for spatial navigation, memory, and social behavior[25,26]. It is noteworthy that the vSub has been shown to regulate specific feeding behaviors driven by environmental context, implying that it integrates sensory cues to regulate food intake[27]. However, whether the vSub can transduce olfactory cues to regulate feeding behavior remains unknown.

Numerous studies have uncovered a key role of the ventral medial hypothalamus (VMH) neurons in energy and glucose homeostasis[28–37]. In particular, chemogenetic activation of VMH neurons inhibits feeding in mice[31,37], while VMH lesions in animals lead to hyperphagia and obesity[38]. Additionally, the VMH integrates sensory information, including olfactory and gustatory cues, which are crucial for feeding behavior and the regulation of metabolic processes[39,40]. A recent study revealed that the paraventricular thalamus (PVT) is one downstream target of the VMH mediating feeding suppression[36]. However, the afferent neural inputs to the VMH that regulate feeding are not fully understood.

In this study, we demonstrate that prolonged exposure to FO suppresses food intake in mice. We found that a subset of neurons in the vSub are activated by FOs but not by the non-food control odors. Using a combination of viral tracing, intersectional genetics, fiber photometry, chemogenetics, optogenetics, and channelrhodopsin-2 (ChR2)-assisted circuit mapping (CRACM), we discovered that FO-activated neurons in the vSub receive glutamatergic projections from the olfactory bulb (OB) and send glutamatergic projections to the VMH. Inhibition of this OB → vSub → VMH circuit abolishes the FO exposure-induced suppression of food intake, while activation of the circuit reduces feeding and body weight. Overall, we identified a FO-responsive neural circuit that is hypophagic and mediates feeding suppression induced by prolonged FO exposure, suggesting a new avenue for treating obesity.

Results

Prolonged FO exposure suppresses feeding

Given evidence for FO exposure decreasing appetite in *Drosophila* and humans, we first asked how FO exposure would impact feeding in mice. To address this question, we established a paradigm that provides an odor-enriched (OE) environment (Fig. 1a). Specifically, holes in the cage bottom for the OE group allowed robust odors to ascend into the cage, while control mice were placed in identical cages without holes, which limited odor detection. Mice were pre-exposed to odors for 30 min before food was provided, and the odor exposure persisted during the food consumption period (Fig. 1a). To generate a robust food odor stimulus transmitted up into the portion of the cage where the mice were located, we utilized a large amount (1 kg) of chow. We found that sustained exposure to this amount of chow-derived odor significantly suppressed chow intake at 1, 2, and 3 h (Fig. 1b). The suppression of food consumption was not observed in mice exposed to acetic acid or isoamyl acetate, two organic odor compounds to which mice show no preference[41] (Supplementary Fig. 1a), suggesting a specific hypophagic response from chow-derived odor. To examine whether the reduced food intake could be attributed to increased foraging, such as increased floor investigation toward the odor source, we analyzed floor-directed exploratory behavior during the first hour of the feeding period using video recordings. Quantification revealed no significant difference in the time spent investigating the floor between OE and control groups (Supplementary Fig. 1b), suggesting that reduced intake is not due to enhanced foraging for the inaccessible odor source. To further validate the observed hypophagic effect, we included an additional control group in which cages had perforated bottoms but no food was placed underneath (Supplementary Fig. 1c). This control ruled out the possibility that control mice detected food odor through residual ambient cues. Consistent with the results in the original setting (Fig. 1b), mice exposed to 1 kg of chow placed under the cage exhibited a significant reduction in food intake compared to those without food odor exposure (Supplementary Fig. 1d). These findings suggests that robust odor exposure, not mere odor detection, is required to drive the hypophagic effect. Supporting this, we found that neither exposure to a small amount (50 g) of chow-derived odor nor a brief exposure period (5 min) to 1 kg chow-derived odor exposure significantly suppressed food intake (Supplementary Fig. 1e, f). We also tested the food intake in mice in the testing cage with or without holes in non-OE condition, and we found no difference in 3-h chow intake (Supplementary Fig. 1g), suggesting that reduced food intake observed using the OE paradigm was not due to discomfort caused by holes in the cage bottom. Together, our findings suggest that FO exposure uniquely suppresses food intake, but the extent of suppression is dependent on both the odor intensity and the duration of exposure.

Given that odor exposure may desensitize the olfactory system to that odor[42], we next assessed if decreased chow intake following prolonged chow-derived odor exposure was confounded by olfactory adaptation. To exclude this possibility, we measured high-fat diet (HFD) intake for mice with or without chow-derived odor-exposed. To reduce the novelty and hedonic drive associated with HFD, mice used in this experiment were acclimated to HFD feeding for 1 week prior to test. We found that mice exposed to chow-derived odor also showed significantly reduced HFD intake (Fig. 1c). Additionally, mice exposed to HFD-derived odor also showed reduced intake of both chow and HFD (Supplementary Fig. 1h), suggesting that FO exposure induces decreased feeding independent of the specific food odor or food. To further determine if reduced food intake was due to FO exposure via olfaction, we established two independent models of anosmia by administering $ZnSO_4$ intranasally[43] or methimazole intraperitoneally[44].

https://doi.org/10.1038/s41467-025-63170-2

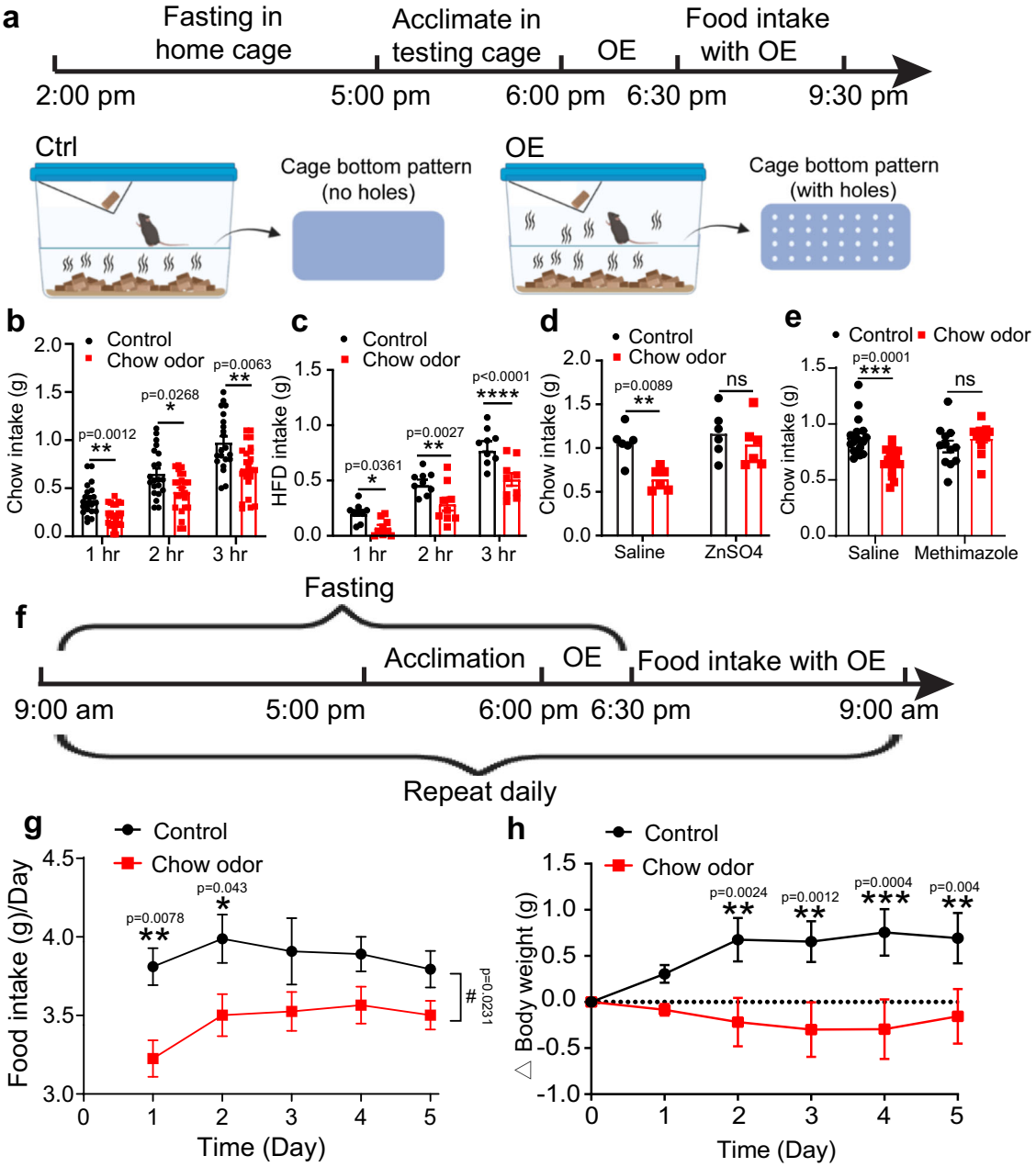

Fig. 1 | Prolong FO exposure suppresses food intake. a Schematic figure for experimental procedure and odor exposure paradigm. **b** Chow intake at 1, 2, 3 h from 6:30 pm to 9:30 pm in chow-fed male mice with or without chow-derived odor exposure. $n = 21$ mice in control group; $n = 23$ mice in chow odor group. **c** HFD intake at 1, 2, 3 h from 6:30 pm to 9:30 pm in HFD-fed male mice with or without chow-derived odor exposure. $n = 9$ mice per group. **d** Three-hour chow intake from 6:30 pm to 9:30 pm in chow-fed male mice treated with saline or $ZnSO_4$. $n = 6$ mice per group. **e** Three-hour chow intake from 6:30 pm to 9:30 pm in chow-fed male mice treated with saline or methimazole. $n = 18$ mice in saline group and 12 mice in methimazole group. **f** Schematic figure for experimental procedure for repeated odor exposure. **g** Daily food intake (6:30 pm–9:00 am) in chow-fed male mice with or without repeated chow-derived odor exposure for 5 days. $n = 5$ mice per group. **h** Body weight change in chow-fed male mice with or without chow-derived odor exposure for 5 days. $n = 5$ mice per group. Two-way ANOVA with *post hoc* Sidak's multiple comparisons in (**b**–**e**). Two-way Repeated Measures ANOVA with *post hoc* Sidak's multiple comparisons in (**g**, **h**). Effect of Chow odor in (**g**), $F_{(1, 8)} = 7.861$, $^{\#}P < 0.05$; $^{*}P < 0.05$, $^{**}P < 0.01$, $^{***}P < 0.001$, $^{****}P < 0.0001$. Data are presented as mean ± SEM with individual data points in (**b**–**e**), and as mean ± SEM in (**g**, **h**). Source data are provided as a Source data file. The Schematics in (**a**) created in BioRender. He, Y. (2025) https://BioRender.com/95d0bwl.

The loss of olfaction in both models was confirmed using a buried food test, in which treated mice showed significantly prolonged latency to locate hidden food (Supplementary Fig. 1i, j). We then tested food intake in these mice using the same paradigm (Fig. 1a). Notably, neither $ZnSO_4$- nor methimazole-treated mice exhibited a significant reduction in food intake when exposed to chow-derived odor (Fig. 1d, e). Importantly, the basal level of food intake under control (non-odor-exposed) conditions before the test did not differ between anosmic mice and their respective control groups, indicating that the lack of FO-induced hypophagia is not due to a compensatory effect of anosmia (Supplementary Fig. 1k, l). We also investigated the long-term impact of sustained FO exposure on feeding and body weight by subjecting mice to repeated daily overnight odor exposures over a 5-day period (Fig. 1f). Compared to controls, mice exposed to chow-derived odor consistently consumed less food overnight each day (Fig. 1g). This persistent hypophagic response was accompanied by a

gradual and significant less body weight gain relative to controls (Fig. 1h). Collectively, these results indicate that FO exposure suppresses food intake in mice via olfaction-mediated pathways.

A vSub → VMH circuit mediates FO exposure-induced hypophagia

Having shown that prolonged FO exposure-induced hypophagia via olfactory inputs, we next sought to investigate the central mechanism underlying this phenomenon. To this end, we first analyzed the expression of the immediate early gene marker c-Fos following odors exposure without food consumption to identify neural ensembles that are activated by FO (Fig. 2a). Consistent with previous findings[45], we observed significantly elevated c-Fos expression in the piriform cortex, a primary olfactory processing region in mammals, following exposure to chow, acetic acid, or isoamyl acetate odors. The magnitude of c-Fos expression was comparable across odor types (Supplementary Fig. 2a, b), indicating that our odor exposure paradigm effectively and sufficiently activates olfactory-involved neural pathways. Notably, we found that mice exposed to chow-derived odor for 1 h showed significantly increased c-Fos expression in the vSub when compared to mice in the control group or those exposed to isoamyl acetate or acetic acid (Fig. 2b, c). To examine whether a brief FO exposure induces activation in the vSub, we performed an additional experiment in which mice were exposed to 1 kg of chow-derived odor for only 5 min, followed by tissue collection at the same time point used for the prolonged exposure condition. We found that brief exposure to chow-derived odor for 5 min failed to increase c-Fos expression in the vSub (Supplementary Fig. 2c). These findings suggest that vSub neurons are selectively and duration-dependently activated by prolonged FO exposure.

Having identified that the vSub is preferentially activated by food-related odors, with minimal responses to non-food odors, we next sought to identify its downstream target. Towards this, we performed channelrhodopsin-2(ChR2)–assisted circuit mapping (CRACM) by injecting adeno-associated viral (AAV) vector carrying ChR2-EYFP into the vSub of WT mice (Fig. 2d, e). We observed abundant EYFP-positive fibers in the VMH (Fig. 2e). While dense EYFP-labeled fibers were concentrated in the shell of the VMH, considerable EYFP-labeled terminals were also detected in the VMH core region (Fig. 2f). To further confirm the projection from the vSub to VMH, we performed CRACM using SF-1-Cre/ Rosa26-LSL-tdTomato mice in which tdTomato-labeled SF-1 neurons in the VMH are mostly distributed in the core region of the VMH (Supplementary Fig. 3a–d). We observed substantial EYFP-positive fibers in the shell of the VMH and dense EYFP-positive terminals in the core region (Supplementary Fig. 3c, d). To verify the projection pattern, we performed retrograde tracing by injecting a retrograde AAV-Cre virus into the VMH and a Cre-dependent mCherry AAV virus into the vSub (Supplementary Fig. 3e), specifically labeling vSub neurons projecting to the VMH with mCherry. Indeed, we observed abundant mCherry-positive neurons in the vSub and mCherry-positive fibers in the VMH (Supplementary Fig. 3g, h), confirming that vSub neurons send projections to VMH. mCherry-positive fibers were also present in the lateral septum (LS) and the nucleus accumbens shell (NAcSh) (Supplementary Fig. 3i, j), suggesting that VMH-projecting neurons also send collateral projections to these areas. Notably, triple RNAscope for *mCherry*, *Vglut2*, and *Vgat* revealed that all of the *mCherry*$^+$ neurons in the vSub express *Vglut2* but not *Vgat* (Supplementary Fig. 3k–n), indicating that VMH-projecting vSub neurons are glutamatergic.

To explore functional connectivity of glutamatergic vSub neurons projecting to the VMH, we expressed ChR2 in glutamatergic vSub neurons by injecting CaMKII-ChR2-EYFP virus into the vSub and then conducting slice electrophysiology recordings from those neurons. We found that photostimulations (473 nm, 5 ms/pulse) elicited robust postsynaptic currents in most (31 out of 35) of the recorded neurons located in the core region of the VMH (Fig. 2g), where neurons are predominantly glutamatergic[46]. We also recorded SF-1 neurons, which are mostly located in the core region of the VMH, using SF-1-Cre/ Rosa26-LSL-tdTomato mice, and we found that all the recorded SF-1 neurons (20 out of 20) responded to photostimulation (Supplementary Fig. 3o), confirming that the neurons in the core region of the VMH are innervated by VMH-projecting vSub neurons. The evoked currents persisted in the presence of tetrodotoxin (TTX) and 4-aminopyridine (4-AP) but were blocked by α-amino-3-hydroxy-5-methyl-4-isoxazolepropionic acid (AMPA) glutamate receptor antagonist 6,7-dinitroquinoxaline-2,3-dione (DNQX) (Fig. 2g and Supplementary Fig. 3o), confirming that the currents were monosynaptic excitatory postsynaptic currents (EPSCs). To determine whether vSub input also targets other hypothalamic cell types, we recorded from GABAergic neurons (15 cells) in the VMH shell using Vgat-Cre/Rosa26-LSL-tdTomato mice and proopiomelanocortin (POMC) neurons (18 cells) in the arcuate nucleus (ARH) using POMC-Cre^{ERT2}/Rosa26-LSL-tdTomato mice; none of these neurons exhibited detectable EPSCs in response to blue light stimulation (Supplementary Fig. 3p, q). Together, these data in both anatomy and functionality demonstrate that glutamatergic neurons in the vSub provide monosynaptic glutamatergic inputs to the VMH.

Having demonstrated functional connectivity, we next examined whether VMH-projecting vSub neurons respond to FO by conducting in vivo fiber photometry recordings from these neurons in freely moving mice. Toward this, we stereotaxically injected a retrograde AAV vector carrying Cre into the VMH, and a Cre-dependent AAV vector carrying GCaMP6m into the vSub and implanted an optic cannula over the vSub (Fig. 2h). We confirmed expression of GCaMP6m in the vSub region (Supplementary Fig. 4a). During the recordings, mice were allowed to freely move in an open cage (40 cm L × 30 cm W × 40 cm H) with 5 cm deep of clean bedding. Small bedding patches (~1 g) infused with different odors: chow, isoamyl acetate, or acetic acid, were placed on the surface of the clean bedding in visually indistinguishable locations. This design ensured that mice could not use visual cues to discriminate odor sources and instead relied on olfactory-guided exploration (Fig. 2i). Fiber photometry recordings revealed a robust and selective increase in calcium activity in VMH-projecting vSub neurons when mice sniffed toward chow-derived odor. In contrast, sniffing spots enriched with isoamyl acetate or acetic acid elicited minimal calcium responses (Fig. 2j). Quantitative analysis confirmed that the peak calcium response to chow odor was significantly greater than the responses to isoamyl acetate or acetic acid odor (Fig. 2k), indicating that VMH-projecting vSub neurons are selectively activated by FO. To strengthen these findings, we conducted an additional experiment using a 4-odor choice design in which mice could smell chow, HFD, isoamyl acetate, and acetic acid odors presented simultaneously (Supplementary Fig. 4b). Consistently, we observed a dramatic increase in calcium activity when mice sniffed toward chow or HFD-derived odor, while responses to isoamyl acetate and acetic acid remained minimal (Supplementary Fig. 4c, d), demonstrating that vSub → VMH neurons are selectively activated by food-derived odors. To assess whether this neural response is maintained over longer durations relevant to the behavioral suppression of feeding, we performed extended fiber photometry recordings during a 30-min continuous exposure to chow-derived odor. We observed an overall elevation in calcium activity relative to baseline that persisted throughout the exposure window, as measured by area under the curve (AUC) analysis (Fig. 2l, m). These data suggest that vSub neurons can remain engaged during prolonged FO exposure, consistent with a role in mediating sustained feeding suppression. Notably, we observed that calcium activity in these neurons was moderately suppressed during active food consumption (Supplementary Fig. 4e). This shift in neural activity across different phases of feeding may reflect distinct, phase-specific roles of the vSub in regulating feeding behavior. This

https://doi.org/10.1038/s41467-025-63170-2

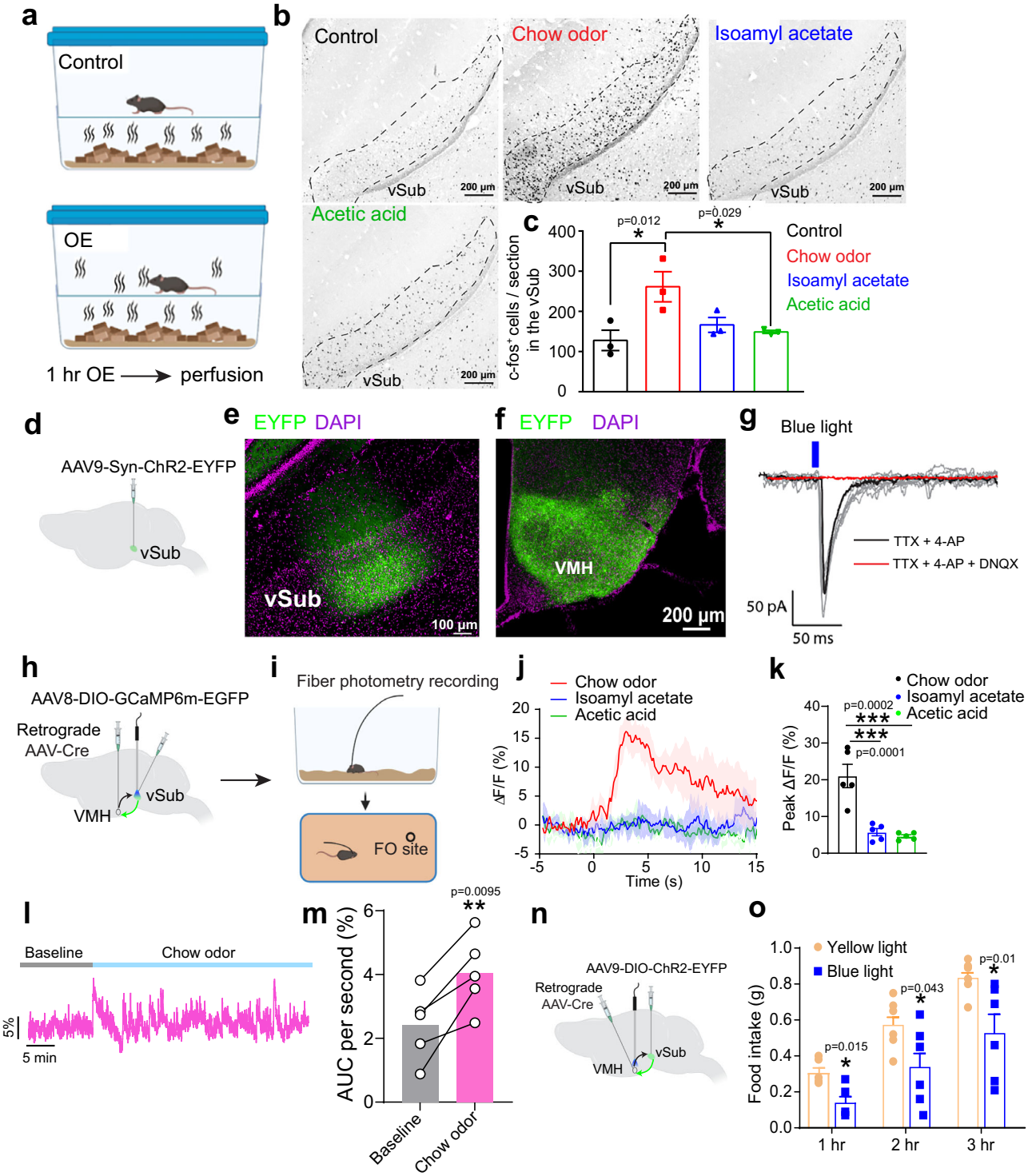

Fig. 2 | A vSub → VMH circuit mediates FO exposure-induced hypophagia. **a** Experimental scheme. **b** Representative c-Fos images in the vSub from mice exposed to odors from Ctrl, chow, isoamyl acetate, and acetic acid. **c** Quantification of c-Fos$^+$ cells in (**b**). $n = 3$ mice per group. **d** Scheme for virus injection in the vSub. Representative images of virus expression in the vSub (**e**) and fibers in the VMH (**f**). **g** Representative traces of blue light-evoked postsynaptic current in VMH neurons in the core region in the presence of TTX and 4-AP (black) and DNQX (red). **h** Scheme for virus injection in the vSub and VMH of WT mice. **i** Experimental scheme. GCaMP6m signals aligned to odor sniffing events (**j**) and quantification of peak ΔF/F% response (**k**) in VMH-projecting vSub neurons in response to odors from chow, isoamyl acetate, and acetic acid. $n = 4$ mice per group. **l** Representative trace of GCaMP6m signals in long-term recordings during baseline and 30-min chow odor exposure. **m** Quantification of area under the curve (AUC) per second during baseline and chow odor exposure. $n = 5$ mice per group. **n** Scheme for virus injection in the vSub and VMH of WT mice. **o** Chow intake at 1, 2, 3 h from 6:30 pm to 9:30 pm in chow-fed male mice with yellow or blue light stimulation. $n = 6$ mice per group. One-way ANOVA with *post hoc* Dunnett's test in (**c**, **k**); Paired two-tailed t-tests in (**m**). Two-way ANOVA with *post hoc* Sidak's multiple comparisons in (**o**). $^*P < 0.05$, $^{**}P < 0.01$, $^{***}P < 0.001$. Data are presented as mean ± SEM in (**j**), and as mean ± SEM with individual data points in (**k**, **o**). Source data are provided as a Source data file. The Schematics in (**a**, **d**, **h**, **i**, **n**) were created in BioRender. He, Y. (2025) https://BioRender.com/j1lhtgr.

dynamic pattern suggests that vSub activity is elevated during food odor detection, which leads to the suppression of feeding in contexts of prolonged odor exposure, and is reduced once consumption begins, possibly to disengage inhibitory signals and permit consummatory behavior. Together, these findings highlight a flexible, stage-specific role for the vSub in modulating feeding across anticipatory and consummatory phases.

The vSub → VMH circuit is both necessary and sufficient to suppress food intake

In order to assess if this food odor-responsive vSub → VMH circuit (Fig. 2) was driving the observed suppressed food intake (Fig. 1), we artificially activated this circuit with ChR2-based in vivo optogenetics by injecting a retrograde Cre virus into the VMH, and a Cre-dependent ChR2 virus into the vSub. An optic fiber was implanted over the VMH of WT mice (Fig. 2n). Cell body expression of ChR2 and abundant ChR2-positive fibers were confirmed in the vSub and VMH regions, respectively (Supplementary Fig. 4f, g). Consistent with previous observation (Supplementary Fig. 3g–j), ChR2-positive fibers were also present in the lateral septum (LS) and the nucleus accumbens shell (NAcSh) (Supplementary Fig. 4h). Slice electrophysiology recordings confirmed functional activation of neurons in the VMH reflected by significantly increased membrane potential and action potential (AP) firing frequency upon photostimulations (Supplementary Fig. 4i–k). To further characterize the postsynaptic targets of the vSub → VMH circuit, we performed triple RNAscope analysis for *Fos*, *Vglut2*, and *Vgat* following chemogenetic activation of VMH-projecting vSub neurons (Supplementary Fig. 4l, m). We observed a significant increase in *Fos* expression in *Vglut2*$^+$ neurons in the VMH of hM3Dq-expressing mice compared to control mice treated with CNO (Supplementary Fig. 4n, p). In contrast, *Fos* expression in *Vgat*$^+$ neurons was sparse and did not differ between groups (Supplementary Fig. 4o, q). These results, together with the electrophysiological data, indicate that activation of vSub inputs selectively engages glutamatergic neurons in the VMH.

Behaviorally, we found that in vivo photostimulation (473 nm, 20 s^{-1}, 10 ms, 1 s on, 2 s off for 3 h) of ChR2-positive vSub neuron fibers within the VMH significantly suppressed food intake (Fig. 2o), indicating that activation of the vSub → VMH circuit suppresses feeding. Given that the vSub is involved in the regulation of stress and anxiety[18], which can influence eating behavior[47], we sought to determine whether activation of the vSub → VMH circuit carries emotional valence. Negative valence typically associated with aversive or anxiety-inducing experiences that could confound the observed suppression of food intake. To assess this, we conducted a real-time place avoidance test in which photostimulation was paired with one-half of an two-chamber arena, an assay commonly used to infer emotional valence: avoidance of the stimulated zone would suggest negative valence (i.e., the stimulation is aversive), whereas preference would indicate positive valence. We found that photostimulation of the vSub → VMH circuit did not induce avoidance of the light-on side (Supplementary Fig. 4r, s), nor did it significantly alter overall locomotor activity or velocity (Supplementary Fig. 4t, u), indicating that the circuit activation does not carry aversive or anxiogenic valence, suggesting that activation of the vSub → VMH circuit does not transduce aversive valence signals. These findings indicate that the reduced food intake observed upon stimulation is not due to stress, anxiety but instead reflects a direct regulatory role of this circuit in feeding behavior.

As we previously showed that VMH-projecting vSub neurons also send collateral projections to the LS and NAcSh (Supplementary Figs. 3g–j and 4h), two brain regions also implicated in the regulation of feeding[48,49], we next asked if the observed reduction in food intake could be mediated by parallel activation of these additional projections. To test this possibility, we performed reciprocal optogenetic and chemogenetic experiments to simultaneously activate VMH-projecting vSub neurons while inhibiting downstream targets in the VMH, LS, and NAcSh, respectively. For this, we delivered retrograde AAV-Cre virus into the VMH and Cre-dependent AAV (AAV9)-ChR2 virus into the vSub in three groups of WT mice. This combination led to the expression of ChR2 in VMH-projecting vSub neurons. In the same mice, we delivered an anterograde trans-synaptic AAV1 vector carrying Flpo into the vSub and a Flpo-dependent AAV (AAV8) virus carrying an inhibitory designer receptor exclusively activated by designer drugs (hM4Di) into either the VMH, LS, or NAcSh (1 node per group of mice) (Fig. 3a). This protocol induced expression of hM4Di only in VMH, LS, or NAcSh downstream neurons innervated by vSub neurons. In the same surgery, an optic fiber was implanted over the vSub. We confirmed the expression of hM4Di and observed ChR2-positive fibers in the VMH (Fig. 3b), LS (Fig. 3h), and NAcSh (Fig. 3k). Slice electrophysiology recordings demonstrated that application of clozapine N-oxide (CNO) effectively abolished photostimulation-induced activation of vSub-innervated VMH neurons (Fig. 3c–e), confirming the functionality of the reciprocal excitatory and inhibitory setup. Importantly, inhibition of vSub-innervated neurons in the VMH significantly attenuated the reduced food intake caused by photostimulation of VMH-projecting vSub neurons (Fig. 3f). In contrast, inhibition of vSub-innervated neurons in the LS (Fig. 3i) or NAcSh (Fig. 3l) did not produce this effect, suggesting that reduced food intake was primarily mediated by vSub projections within the VMH.

In order to determine the necessity of the vSub → VMH circuit in mediating FO-induced hypophagia, we employed Arch3.0-based in vivo optogenetics to inhibit VMH-projecting neurons in the vSub region by bilaterally injected a retrograde Cre virus into the VMH, and a Cre-dependent Arch3.0 virus into the VMH. Two optic fibers were implanted over the bilateral vSub (Fig. 4a). The expression of Arch3.0 (Fig. 4b) and functional inhibition of VMH-projecting vSub neurons were confirmed (Fig. 4c–e). We found that photostimulation with yellow light (596 nm, 20 s^{-1}, 5 ms, 1 s on, 2 s off for 3 h) to inhibit VMH-projecting vSub neurons largely blunted FO-suppressed food intake (Fig. 4f), suggesting that the vSub → VMH circuit is required for FO-induced hypophagia. To further dissect the specific contributions of the vSub → VMH circuit in mediating FO-induced hypophagia compared to collateral projections to the LS and the NAcSh, we measured food intake in mice exposed to prolonged FO exposure (Fig. 4g) while selectively inhibiting vSub-innervated neurons in the VMH, LS, or NAcSh. Toward this, we utilized mice from the reciprocal experiment in which inhibitory hM4Di receptors were expressed in the vSub-innervated neurons within the VMH, LS, or NAcSh. These mice were injected with saline or CNO, followed by FO exposure and food intake measurement (Fig. 4g). Only inhibition of vSub-innervated VMH neurons significantly attenuated FO-induced hypophagia (Fig. 4h–j). Together, these results demonstrate that the vSub → VMH circuit is both necessary and sufficient for FO-induced hypophagia.

OB is the upstream node of the vSub → VMH circuit that mediates FO-induced hypophagia

Next, we aimed to identify the upstream neural inputs of VMH-projecting vSub neurons. Toward this, we used the TRIO (Tracing the Relationship between Input and Output) strategy using a modified monosynaptic rabies virus system. Briefly, we delivered a retrograde Cre virus into the VMH, while the vSub received the Cre-dependent helper virus (AAV8-DIO-GTB), which co-expresses the rabies glycoprotein (RG) and the avian TVA receptor. This allowed RG and TVA expression specifically in VMH-projecting vSub neurons. Three weeks later, we injected the G-deleted, pseudotyped rabies virus (EnvA-ΔG-Rabies-GFP) into the vSub to infect helper+ VMH-projecting vSub neurons via their presynaptic terminals (Fig. 5a, b). In alignment with previous observations[17], GFP-positive neurons were detected in the nucleus of Diagonal band of Broca (DBB) and the paraventricular thalamus (PVT) (Supplementary Fig. 5a, b). Remarkably, we found that

https://doi.org/10.1038/s41467-025-63170-2

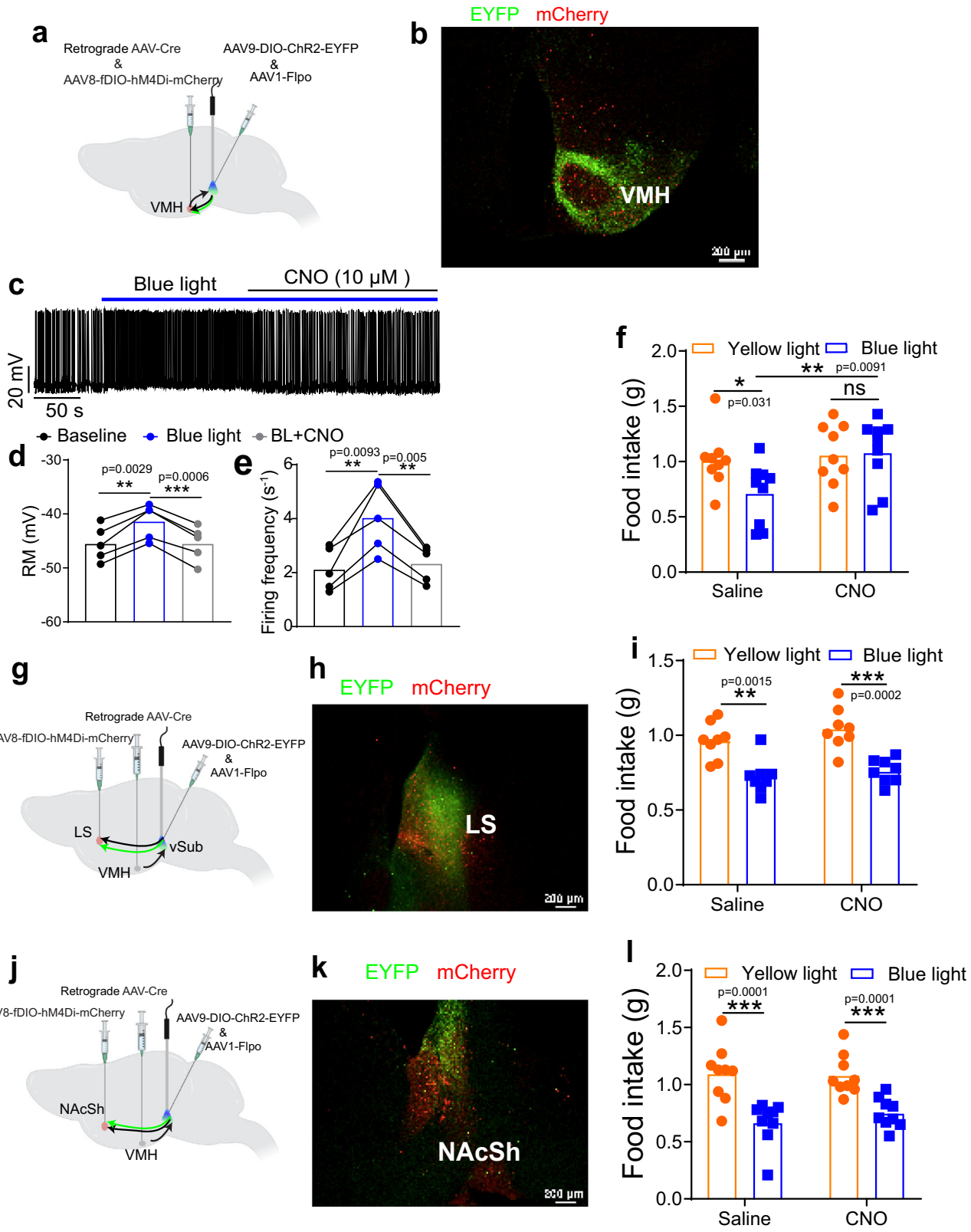

a subset of neurons located in the granular cell layer of accessory olfactory bulb (GrA) in the OB were labeled by GFP (Fig. 5c), indicating a synaptic connection between OB neurons and vSub neurons that project to the VMH. Given that the OB is a pivotal hub for transmitting smell information from the nose to the brain, and we revealed that disruption of olfaction by intranasal application of $ZnSO_4$ or i.p. injection of methimazole abolishes FO-suppressed food intake, these tracing data imply that OB may be the key upstream node of the vSub → VMH circuit that mediates FO-induced hypophagia.

To confirm the synaptic connectivity between the OB and the vSub, we stereotaxically injected a retrograde AAV vector carrying Cre into the vSub, and a Cre-dependent AAV vector carrying ChR2-EYFP into the OB (Fig. 5d). The expression of ChR2 in the OB was confirmed (Fig. 5e) and EYFP-positive fibers were detected in the vSub

Fig. 3 | Reciprocal opto/chemogenetic manipulation of collateral projections of VMH-projecting vSub neurons. a Scheme for virus injection in the vSub and VMH of WT mice. **b** Validation of the expression of hM4Di and ChR2-positive fibers in the VMH. Representative trace showing action firing potential changes in VMH neurons with blue light stimulation and CNO treatment in slice electrophysiology recordings (**c**), and quantification of the membrane potential (**d**) and firing frequency (**e**). $n = 5$ neurons per group. **f** Three-hour chow intake in chow-fed male mice from 6:30 pm to 9:30 pm with saline or CNO treatment upon yellow or blue light stimulation. $n = 9$ mice per group. **g** Scheme for virus injection in the vSub and LS of WT mice. **h** Validation of the expression of hM4Di and ChR2-positive fibers in the LS. **i** Three-hour chow intake in chow-fed male mice from 6:30 pm to 9:30 pm with saline or CNO treatment upon yellow or blue light stimulation. $n = 8$ mice per group. **j** Scheme for virus injection in the vSub and NAcSh of WT mice. **k** Validation of the expression of hM4Di and ChR2-positive fibers in the NAcSh. **l** Three-hour chow intake in chow-fed male mice from 6:30 pm to 9:30 pm with saline or CNO treatment upon yellow or blue light stimulation. $n = 9$ mice per group. Paired two-tailed t-tests in (**d**, **e**). Two-way ANOVA with *post hoc* Sidak's multiple comparisons in (**f**, **i**, **l**). $^{*}P < 0.05$, $^{**}P < 0.01$, $^{***}P < 0.001$. Data are presented as mean ± SEM with individual data points. Source data are provided as a Source data file. The Schematics in (**a**, **g**, **j**) were created in BioRender. He, Y. (2025) https://BioRender.com/jot50le.

(Supplementary Fig. 5c). In slice electrophysiology recordings in vSub neurons, we observed that photostimulation (473 nm, 5 ms/pulse) elicited excitatory postsynaptic currents (EPSCs) in recorded neurons (6 of 10 neurons) in the vSub (Fig. 5f). These evoked EPSCs persisted in the presence of 4-AP and TTX (Fig. 5f), indicating that the recorded neurotransmissions are likely monosynaptic. Additionally, all evoked EPSCs were blocked by the AMPA glutamate receptor antagonist DNQX (Fig. 5f), confirming that recorded EPSCs were glutamatergic. Thus, these data indicate that the OB provides monosynaptic glutamatergic inputs to the vSub.

Next, we sought to determine whether inhibition of the OB → vSub circuit impedes FO-induced hypophagia. To address this question, we expressed a mutated Kir2.1 channel, an inward-rectifier potassium ion channel that hyperpolarizes neurons[50], in vSub-projecting OB neurons by injecting retrograde AAV vector carrying Cre into the bilateral vSub and a Cre-dependent AAV (AAV9) vector carrying Kir2.1-tdTomato into the bilateral OB (Fig. 5g, h). In control mice, the AAV vector carrying Kir2.1-tdTomato was substituted with a vector carrying tdTomato alone. In agreement with previous findings[50], slice electrophysiology recordings showed that neurons expressing Kir2.1 exhibited significant lower membrane potential and higher AP firing threshold (Supplementary Fig. 5d–g), confirming an inhibitory effect in vSub-projecting OB neurons. In a single-exposure FO paradigm, exposure to chow-derived odor significantly suppressed food intake in control mice; in contrast, Kir2.1 mice showed comparable food intake in response to chow-derived odor exposure compared to non-odor condition (Fig. 5i). To examine whether this circuit is also required for prolonged FO-induced suppression, we subjected Kir2.1 and control mice to a repeated odor exposure protocol described in Fig. 1f. In contrast to control mice, which exhibited daily hypophagia and suppressed body weight gain over 5 days, Kir2.1 mice displayed significantly higher food intake and greater body weight gain during the odor exposure period (Fig. 5j, k), while the baseline food intake and body weight in Kir2.1 mice are comparable with control mice (Supplementary Fig. 5h, i). These results support that the OB is the upstream node of the vSub → VMH circuit that mediates FO-induced hypophagia.

Constant activation of the OB → vSub circuit reduces food intake and body weight

It has been reported that enhancement of OSN signaling leads to a reduction in feeding in *Drosophila*[13]. In our study, we also observed that repeated and constant exposure to FO suppresses body weight gain in mice. We next interrogated whether constant activation of the vSub-projecting OB neurons decreases both food intake and body weight, which mimics the effect of prolonged and sustained exposure to FO. To this end, we expressed NaChBac, a bacterial sodium channel known for its ability to constantly increase neuronal activity[50], in vSub-projecting OB neurons by delivering retrograde AAV vector carrying Cre into the vSub, and a Cre-dependent AAV (AAV-DJ) vector carrying NaChBac-GFP into the GrA of OB (Fig. 6a). In control mice, the AAV vector carrying NaChBac-GFP was substituted with a vector carrying GFP alone. The expression of GFP was confirmed in the OB (Fig. 6b). Slice electrophysiology recordings showed that NaChBac-expressing neurons exhibited lower firing threshold and wider action firing potential width (Fig. 6c–f), indicating increased neural activity and excitability in vSub-projecting OB neurons. Notably, chronic activation of vSub-projecting OB neurons by NaChBac significantly reduced body weight gain and food intake under both chow and HFD diet feeding (Fig. 6g–j). The reduced body weight under HFD feeding was solely due to decreased fat accumulation (Fig. 6k, l). These data indicate that constant activation of the OB → vSub circuit suppresses feeding and attenuates diet-induced obesity.

Discussion

Here, we demonstrated that prolonged FO exposure suppresses feeding in mice via a mechanism in which FO activates excitatory inputs from the OB to the vSub that send glutamatergic projections to the VMH. Inhibiting the OB → vSub → VMH circuit abolished the FO-induced reduction in food intake, while activating this circuit suppressed feeding and reduced body weight. Collectively, our study unveils an OB-originating neural circuitry involving the vSub and the VMH that mediates the suppression of food intake induced by prolonged exposure to food-derived odors.

Appetite suppression by food odors is a known phenomenon in humans[9,12,14]. A study in *Drosophila* also showed a reduced food intake upon sustained food odor exposure[13]. However, this phenotype has not been thoroughly investigated using mouse model, which possesses similar olfactory system with humans[51]. In the present study, we discovered that feeding was suppressed in mice exposed to both chow and HFD-derived odor prior to consumption of food using a sophisticated odor exposure paradigm. Interestingly, a recent study reported that olfactory cues of food odor are neither necessary nor sufficient to alter feeding patterns regardless of hunger state[52]. The discrepancies between this study and our findings could be attributed to differences in methodology. The previous study used a porous, opaque tea ball containing small amounts of HFD placed in the food wire at the top of the cage, which might not have produced a strong enough odor to affect food intake. Indeed, reduced food intake was not observed with either minimal FO exposure or brief exposure periods in our study, suggesting that both the quantity of odor and the duration of exposure are critical factors. Nonetheless, we acknowledge that our experimental design has certain limitations. For example, the food pellet provided for consumption at the top of the cage during the test period could itself emit odor, which may contribute to the overall olfactory environment. While the control cages were designed without holes to limit odor diffusion, it remains possible that mice with intact olfaction could detect faint residual cues, given their highly sensitive olfactory system. However, our additional control group using perforated cages without food beneath showed consistent feeding phenotype, arguing against meaningful behavioral effects from low-level ambient odor. While we did not directly measure odorant concentration or test a full range of intermediate food quantities (e.g., 250 g or 500 g), our findings from two extremes (50 g and 1 kg) support the existence of a functional threshold for

https://doi.org/10.1038/s41467-025-63170-2

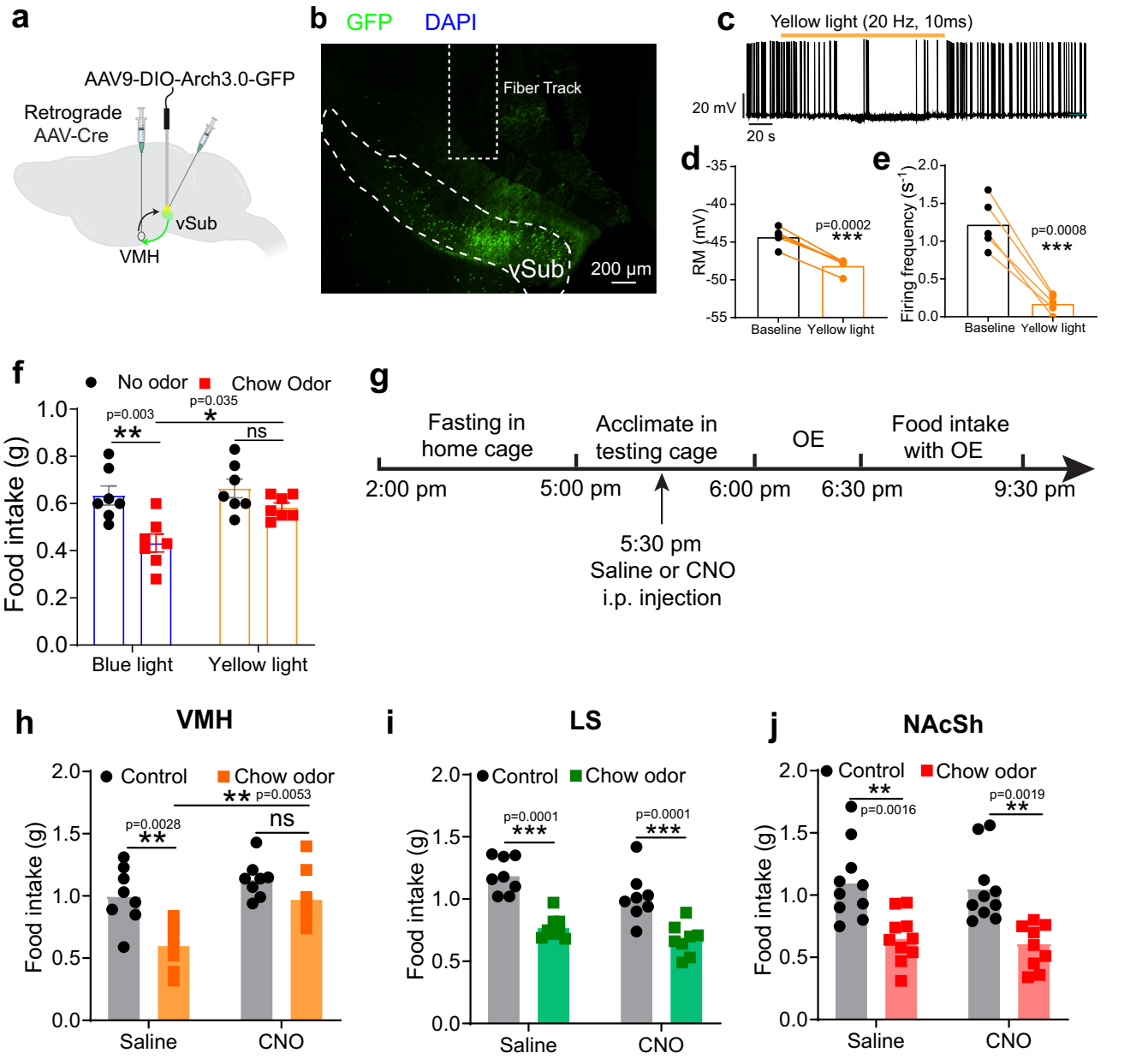

Fig. 4 | Inhibition of vSub → VMH circuit attenuated FO-induced hypophagia. **a** Scheme for virus injection in the vSub and VMH of WT mice. **b** Validation of the expression of Arch in the vSub. Representative trace showing action firing potential changes in VMH-projecting vSub neurons with yellow light stimulation (**c**) and quantification of the membrane potential (**d**) and firing frequency (**e**). $n = 5$ neurons per group. **f** Three-hour chow intake from 6:30 pm to 9:30 pm in mice in Ctrl (no odor) or chow-derived odor exposure group with yellow or blue light stimulation. $n = 7$ mice per group. **g** Schematic figure for experimental procedure and odor exposure paradigm. Three-hour chow intake from 6:30 pm to 9:30 pm with saline or CNO treatment upon non-FO or FO exposure in chow-fed male mice with hM4Di expression in vSub-innervated VMH (**h**), LS (**i**), and NAcSh (**j**) neurons. $n = 8$ mice in (**h**, **i**); $n = 10$ mice in (**j**). Paired two-tailed t-tests in (**d**, **e**). Two-way ANOVA with *post hoc* Sidak's multiple comparisons in (**f**, **h**, **i**, **j**). *P < 0.05, **P < 0.01, ***P < 0.001. Data are presented as mean ± SEM with individual data points. Source data are provided as a Source data file. The Schematics in (**a**) were created in BioRender. He, Y. (2025) https://BioRender.com/2gcdnui.

odor-driven feeding suppression. Moreover, our c-Fos data demonstrate that both odor intensity and exposure duration correlate with activation in FO-responsive circuits, further supporting a threshold-dependent model for odor-induced hypophagia. Consistent with this, our long-term fiber photometry recordings revealed that prolonged exposure to chow-derived odor elicited sustained calcium activity in VMH-projecting vSub neurons. Taken together, while our results strongly support a threshold-dependent effect of odor strength and exposure duration on feeding suppression, future studies using partially isolated compartments may help further dissociate incidental background odor from the targeted stimulus and refine our understanding of how olfactory cues modulate feeding behavior.

Various studies have presented debated conclusions regarding the extent and mechanisms by which olfaction influences eating behavior and subsequent weight change. One study reported that ablation of mature OSNs through the expression of diphtheria toxin receptor in olfactory marker protein (OMP)-expressing Cre adult mice led to hyposmia and resistance to diet-induced obesity, along with increased energy expenditure[53]. However, such metabolic phenotypes were not observed in a recent study where olfactory bulbectomies were performed on 8-week-old adult wild-type mice[52]. Contrary to

https://doi.org/10.1038/s41467-025-63170-2

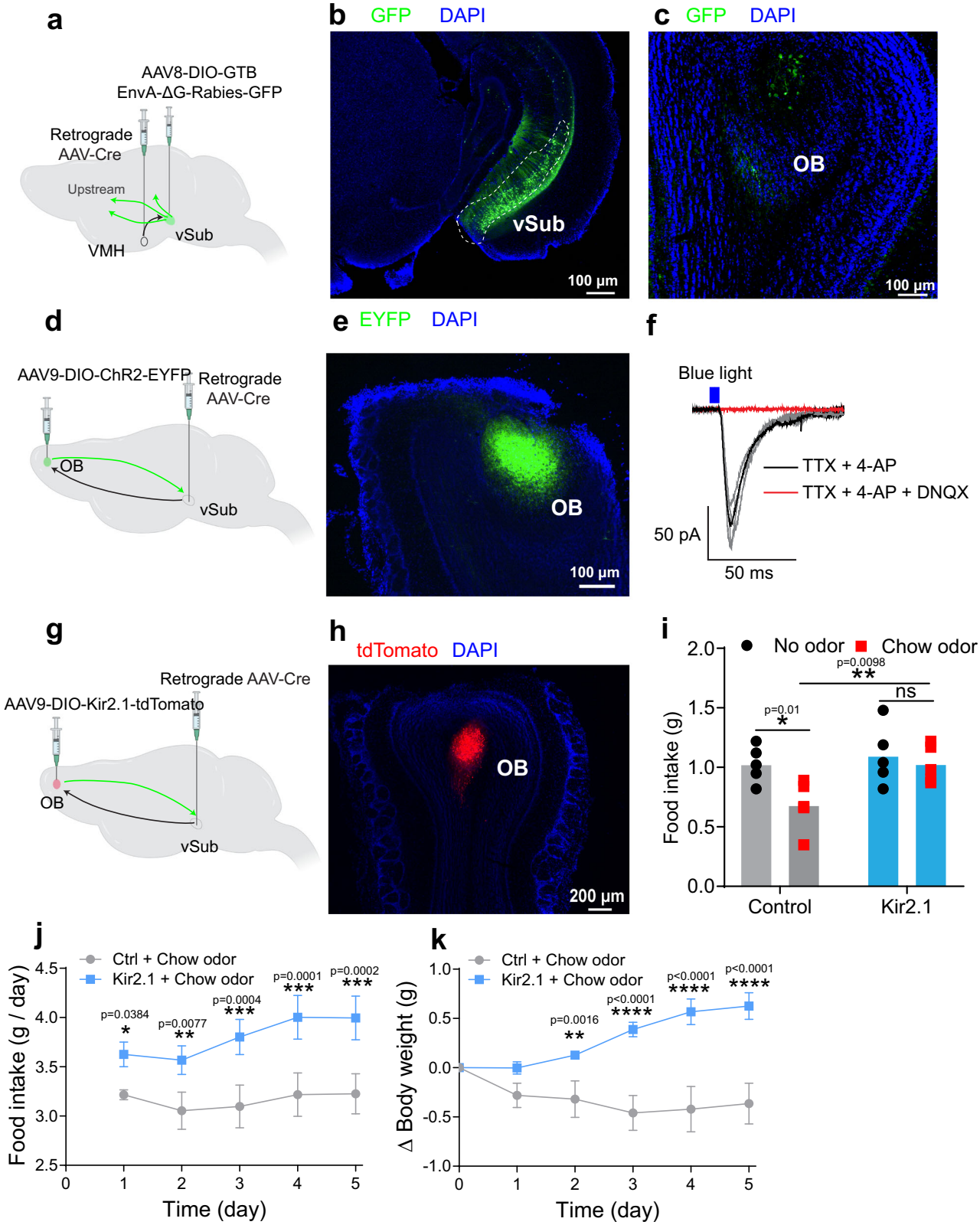

these findings, it has been observed that olfactory bulbectomy produces hyperphagia and obesity in rats and European hamsters[54,55]. Interestingly, the dietary outcomes and body weight changes vary greatly among individuals with olfactory dysfunction in human studies. Some patients with loss of smell tend to eat more and gain more body weight, while others eat less and gain less weight[56]. Given these complex interactions, it is clear that a deeper understanding of the mechanisms in anatomical and cellular levels by which olfaction influences feeding behavior and metabolism is needed. Our findings that constant activation of vSub-projecting OB neurons suppresses feeding and attenuates diet-induced obesity highlight a crucial role of specific neuronal populations within the OB in orchestrating feeding behavior in mice. Consistent with our findings, overexpression of sNPF in OSNs, which leads to the enhancement of OSNs activity, suppresses

https://doi.org/10.1038/s41467-025-63170-2

Fig. 5 | An OB → vSub → VMH circuit mediates FO-induced hypophagia. a Scheme for virus injection in the vSub and VMH of WT mice. Representative images of GFP-labeled starter neurons in the vSub (**b**) and GFP-labeled upstream neurons in the OB (**c**) from three indepent experiments. **d** Scheme for virus injection in the vSub and OB of WT mice. **e** Representative image of virus expression in the OB from three indepent experiments. **f** Representative traces of blue light-evoked postsynaptic current in vSub neurons in the presence of TTX and 4-AP (black) and DNQX (red). **g** Scheme for virus injection in the vSub and OB of WT mice. **h** Representative image of virus expression in the OB with the virus injection in (**g**) from five indepent experiments. **i** Three-hour chow intake from 6:30 pm to 9:30 pm in control and Kir2.1-expressing male mice in control (no odor) or chow-derived odor exposure group. $n = 5$ mice per group. **j** Daily food intake (6:30 pm–9:00 am) in chow-fed control and Kir2.1-expressing male mice with repeated chow-derived odor exposure for 5 days. $n = 5$ mice per group. **k** Body weight change in chow-fed control and Kir2.1-expressing male mice with chow-derived odor exposure for 5 days. $n = 5$ mice per group. Two-way Repeated Measures ANOVA with *post hoc* Sidak's multiple comparisons. *P < 0.05, **P < 0.01, ***P < 0.001, ****P < 0.0001. Data are presented as mean ± SEM with individual data points in (**i**), and as mean ± SEM in (**j**, **k**). Source data are provided as a Source data file. The Schematics in (**a**, **d**, **g**) were created in BioRender. He, Y. (2025) https://BioRender.com/os9kdf6.

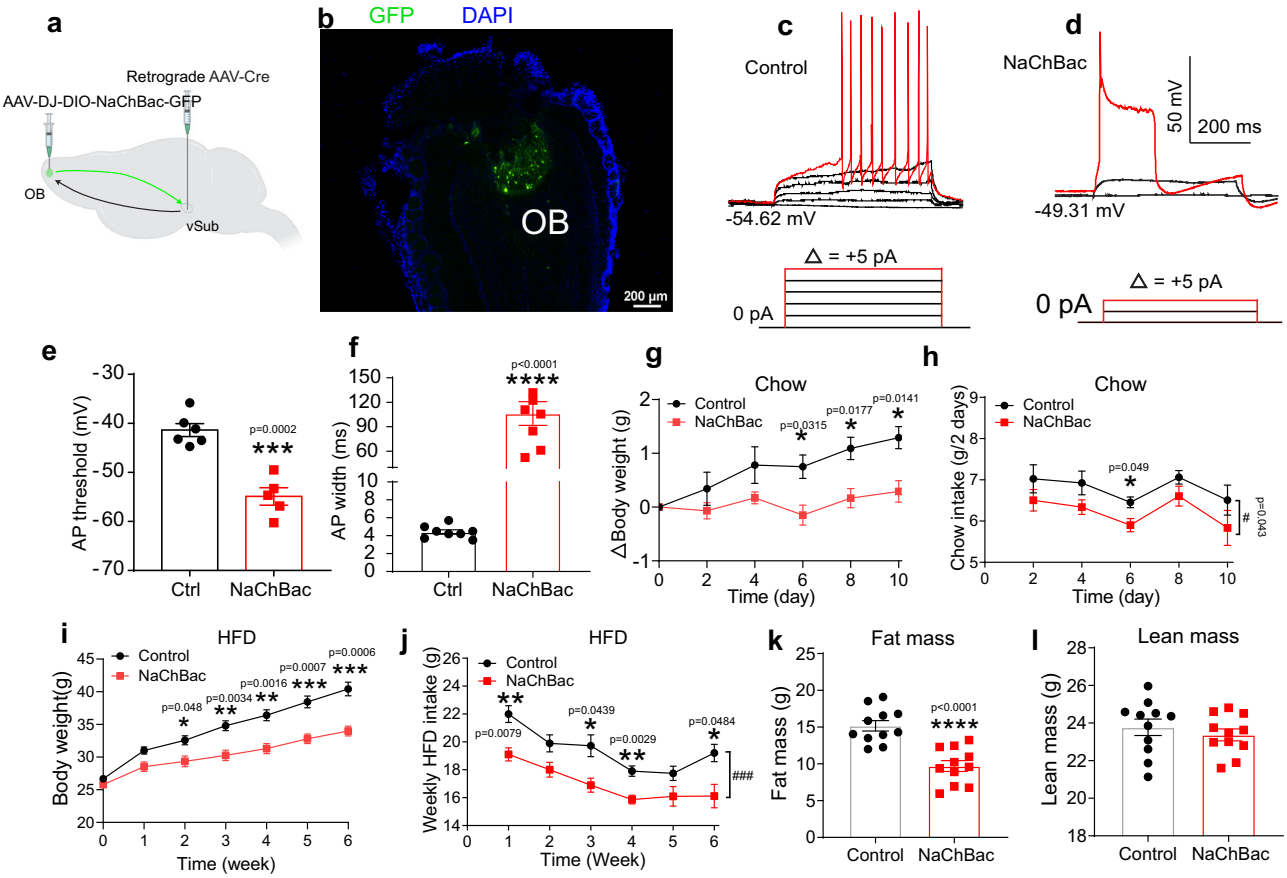

Fig. 6 | Constant activation of vSub-projecting OB neurons suppresses food intake and reduces body weight. a Scheme for virus injection in the vSub and OB of WT mice. **b** Representative images of virus expression in the OB. Representative trace of action potential firing by current injections in a step increment of 5 pA from resting membrane potential in the control (**c**) and NaChBac-expressing (**d**) neurons. **e** The minimum membrane potential required to induce action potential firing in control and NaChBac-expressing neurons in the OB. $n = 6$ neurons in Ctrl group and 5 neurons in NaChBac group. **f** The action potential width in control and NaChBac-expressing neurons in the OB. $n = 8$ neurons per group. Body weight change on chow diet (**g**), bi-daily chow intake (**h**) in the control and NachBac-expressing mice. $n = 11$ mice per group. Body weight on HFD (**i**) and weekly HFD intake (**j**) in the control and NachBac-expressing mice. $n = 11$ mice per group. Fat mass (**k**) and lean mass (**l**) in the control and NaChBac-expressing mice. $n = 11$ mice per group. Unpaired two-tailed t-tests in (**e**, **f**, **k**, **l**). Two-way Repeated Measures ANOVA with *post hoc* Sidak's test in (**g**–**j**). Effect of NaChBac in (**h**), $F_{(1, 20)} = 4.574$, $^{\#}P < 0.05$; Effect of NaChBac in (**j**), $F_{(1, 20)} = 27.44$, $^{\#\#\#}P < 0.001$; *P < 0.05, **P < 0.01, ***P < 0.001, ****P < 0.0001. Data are presented as mean ± SEM with individual data points in (**e**, **f**, **k**, **l**) and as mean ± SEM in (**g**–**j**). Source data are provided as a Source data file. The Schematics in (**a**) were created in BioRender. He, Y. (2025) https://BioRender.com/jlynxc8.

feeding in *Drosophila*[13]. Additionally, deletion of voltage-dependent potassium channel Kv1.3, which depolarizes the mitral cells in the OB, has been associated with enhanced olfactory function[57] and resistance to diet-induced obesity in mice[58]. Future studies are required to elucidate the neural specificity within the OB that mediates FO-induced hypophagia.

Our decision to focus on the vSub was guided by both this selective activation by FO and its known role as a major integrative hub that processes sensory, contextual, and motivational information[24]. Prior studies have implicated the vSub in behavioral valence[20], salience detection[59], and goal-directed behavior[23], making it a strong candidate for relaying food odor signals to downstream circuits that regulate feeding. Our study highlights a population of glutamatergic neurons within the vSub that are activated by FO. While our initial c-Fos mapping was performed using chow-derived odor, our follow-up fiber photometry recordings demonstrate that VMH-projecting vSub neurons are similarly activated by both chow and HFD odors. This broader responsiveness suggests that vSub activation is not restricted to a single olfactory profile, but rather reflects a generalized sensitivity to food-related odors. Supporting this, exposure to HFD also suppressed

food intake in mice. Future studies using mass spectrometry-based volatile profiling could identify the precise odorant molecules present in chow and HFD preparations that drive vSub activation. The vSub contains heterogeneous populations of neurons that are innervated by various upstream brain regions and project to multiple distinct downstream regions to coordinate diverse behaviors, including motivation, reward, stress, anxiety[17,60]. Our findings that the vSub receives direct inputs from the OB expand the existing knowledge of the aggregated neural network from various upstream regions within the vSub, pointing to the sensory responsiveness of this region and its role in modulating feeding behavior. Consistent with previous findings[61], our data show that the VMH serves as a major downstream target of the vSub. Inhibition of the vSub → VMH abolishes the FO-induced hypophagia, while activation of the circuit suppresses food intake. Kosse et al. showed that a small group of BDNF-positive neurons in the VMH sits directly downstream of arcuate AgRP and POMC neurons and projects to jaw premotor centers[62]. Silencing these cells increases feeding, while activating them blocks the orexigenic effect of AgRP stimulation, establishing the VMH as a postsynaptic gatekeeper of consummatory actions driven by interoceptive energy-state signals. Our data extend this model by demonstrating that olfactory food cues recruit a group of VMH ensembles to inhibit food intake, even in the absence of changes in systemic energy state. Together, these findings support a unifying framework in which diverse upstream modalities, including hormonal, metabolic, and sensory, converge on the VMH to modulate food intake. Whether the vSub-innervated VMH neurons correspond molecularly to the VMH^{BDNF} subset described by Kosse et al. remains unknown. Intersectional silencing of VMH^{BDNF} during FO exposure, or single-cell transcriptomic profiling of FO-activated VMH cells, will be able to address this question. Interestingly, despite the involvement of the vSub and VMH in mood regulation and stress responses, which also influences feeding behavior[63], activation of this circuit did not induce alternation in valence in mice, indicating that the observed hypophagia is specific to the sensory and feeding-related pathways without affecting overall mood or emotional states.

In alignment with the existing findings[60,61], our data revealed that VMH-projecting vSub neurons send substantial collateral projections to the NAcSh and LS. We further demonstrated that activation of the entire collateral projections from the vSub to the VMH, LS, and NAcSh by optogenetic excitation of upstream vSub neurons inhibits food intake, whereas reciprocal inhibition of the VMH, but not the NAcSh or the LS, blocks the reduced food intake, indicating the hypophagic effect is mediated by the vSub → VMH circuit. Supporting this, recent work by Wee et al.[64] demonstrated that activity in the vSub → NAcSh pathway increases the probability that a fasted mouse transitions from food investigation to the first feeding bout, but does not alter the total amount of food consumed over longer timescales. These findings are consistent with our results, as we found that manipulating the vSub → NAcSh pathway did not impact overall feeding behavior in our prolonged food access paradigm. Although we did not explore the physiological role of the other two collateral projections, given the involvement of the vSub in diverse functions, these projections to the NAcSh and the LS, two regions highly implicated in the regulation of motivation and stress, might be important for motivation and stress regulation. Indeed, a recent study reported that chemogenetic activation of NAcSh-projecting melanocortin 4 receptor (MC4R)-expressing neurons within the vSub, which also send collateral projections to the VMH and the LS, regulates the eating motivation with mild effect in suppressing homeostatic feeding[61]. It is noteworthy that brain-wide mapping of monosynaptic inputs in this study showed that NAcSh-projecting MC4R-expressing neurons in the vSub do not receive projections from the OB. Such results indicate that vSub-projecting OB neurons that project to the VMH in our study, which are accountable for FO-induced hypophagia, are not MC4R-expressing neurons. Future studies, such as transcriptomic study using single-cell sequencing, are needed to delineate the specific cell types in the vSub that mediate FO-induced suppression of food intake.

In summary, our study reveals a FO-responsive neural circuit involving the vSub and VMH that mediates the suppression of food intake induced by prolonged FO exposure. These findings provide significant insights into the olfactory modulation of feeding behavior and identify potential targets for obesity intervention.

Methods

Mice

C57BL/6J male WT, SF-1-Cre/Rosa26-LSL-tdTomato, POMC-CreERT2/Rosa26-LSL-tdTomato, and Vgat-Cre/Rosa26-LSL-tdTomato mice, aged over 8 weeks, were used in this study. Mice were given *ad libitum* access to water and standard chow diet (6.5% fat, #2920, Harlan-Teklad, Madison, Wisconsin) unless otherwise specified. Mice were housed in a temperature and humidity-controlled environment (temperature 22 ± 1 °C, humidity 50 ± 5%) using a 12-h light and 12-h dark cycle with lights on at 6:00 am and off at 6:00 pm. All experimental procedures followed this schedule. Mice were initially group-housed, and upon surgery or the start of home cage feeding experiments, mice were then single-housed (12:12 h light/dark cycle). For the mice subjected to HFD intake upon chow/HFD-derived odor exposure, mice were fed with HFD (60% fat, #D12492i, Research Diets) for 1 week to reduce the hedonic impact of HFD. Care of animals and procedures were approved by the Baylor College of Medicine Institutional Animal Care and Use Committee.

Odor exposure

A standard chow diet (1 kg or 50 g, depending on the study design) was used to generate chow-derived odor, and an HFD (500 g) was used to generate HFD-derived odor. For exposing mice to the odors from acetic acid and isoamyl acetate, a 10 cm diameter plastic cell culture dish was placed in the lower container, and 10 ml of acetic acid or isoamyl acetate was added to the dish to volatilize and produce the odor.

Food intake, body weight, and body composition

Mice are singly housed and allowed to acclimate for at least 1 week before being subjected to the food intake study. For the 3-h food intake measurement under odor exposure, mice were fasted from 2 pm to 5 pm in their home cage to achieve a comparable metabolic and energy status. Then the mice were subjected to odor exposure paradigm and underwent the procedures indicated in the figure. Pre-weighed food was provided at 6:30 pm, and food intake was measured at 1-h intervals from 6:30 pm to 9:30 pm.

For repeated overnight food intake measurement under odor exposure, mice were fasted from 9:00 am to 5:00 pm in home cage to maintain a comparable metabolic and energy status. Afterward, the mice were subjected to the odor exposure paradigm and underwent the procedures indicated in the figure. Pre-weighed food was provided at 6:30 pm, and food intake and body weight were measured at 9:00 am each day.

For optogenetic study, mice were fasted from 2 pm to 5 pm in their home cage and transferred to the testing cage used for odor exposure study. Chow-derived odor exposure absent in excitatory optogenetic studies and was provided in inhibitory optogenetic studies. Light stimulation (blue or yellow light at 20 Hz, 5 ms/pulse, 1 s on, 2 s off) was applied from 6:30 pm to 9:30 pm when food was provided. Food intake was measured from 6:30 pm to 9:30 pm. The intensity of light pulses (7–8 mW at the fiber tip) was determined based on parameters used in previous studies and measured using an optical power meter (PM20A, Thorlabs).

For the long-term food intake and body weight measurement in mice receiving NaChBac injection, mice are singly housed after recovery for 2 weeks after surgery. Food intake and body weight were

monitored on chow every 2 days and on HFD every week until the end of the study. Body composition was determined by quantitative magnetic resonance.

Anosmia induction and evaluation

The induction of anosmia in mice by intranasal application of zinc sulfate was performed as previously described[43]. Briefly, mice were anesthetized using uniflow nose cone and exposed the snout. Each nostril was injected with 50 µl of a sterile 5% solution of $ZnSO_4$ or with 50 µl of saline. The injections were made by forcefully expelling the contents of a syringe through a blunted 4 mm long 25 G needle inserted ~3 mm into the naris. The first injection was made into the right naris. The left naris was injected 2 h later. Immediately after intranasal $ZnSO_4$ irrigation, the mouse was held with its head down for several seconds to minimize spread of the solution to the oral cavity. After 1 day recovery, the mice were subjected to a 10-min buried food test as previously described[52] to evaluate olfactory function. Briefly, mice were fasted overnight for 16–18 h before experiments. A chow pellet was hidden under the bedding using an acrylic box (40 cm L × 30 cm W × 40 cm H). The latency to food discovery was recorded. To establish another anosmia mouse model, olfactory nerve ablation was induced using methimazole treatment as previously described[65], with intraperitoneal injections of methimazole (50 mg/kg body weight in saline) administered on days 0 and 3 of treatment. After recovery, the mice were subjected to a 10-min buried food test as described above.

Stereotaxic surgery

Mice were anaesthetized (2% isoflurane) and placed in a stereotaxic instrument. Artificial eye ointment was applied to prevent corneal drying, and a heat pad was used to hold body temperature at 37 °C. To specifically identify the downstream targets of vSub glutamatergic neurons, we injected AAV9-hSyn-ChR2 (H134R)-EYFP into the vSub of wild-type mice (Addgene, #26973, titer: 5×10^{12} GC/ml, 0.2 µl/injection; AP: -3.8 mm; ML: ±3 mm; DV: −4.6 mm). To retrogradely label VMH-projecting vSub neurons, we injected retrograde AAV-Cre (Addgene, #105553-AAVrg, titer: 5×10^{12} GC/ml, 0.2 µl/injection) into the VMH (AP: −1.7 mm; ML: 0.5 mm; DV: −5.65 mm), and delivered AAV8-DIO-mCherry (Addgene, #50459, titer: 5×10^{12} GC/ml, 0.2 µl/injection) into the vSub.

To record the response of vSub neurons (that send projections to the VMM) to FO through fiber photometry, we injected retrograde AAV-Cre (Addgene, #105553-AAVrg, titer: 5×10^{12} GC/ml, 0.2 µl/injection) into the VMH, and delivered AAV8-DIO-GCaMP6m (Addgene, #100838, titer: 5×10^{12} GC/ml, 0.2 µl/injection) into the vSub. During the same surgery, an optic fiber (MFC_400/430-0.66, Doric) was placed above the vSub (AP: −3.8 mm; ML: 3 mm; DV: −4.4 mm), fibers were fixed to the skull using dental acrylic.

To uncover the synaptic properties of the $vSub^{VGLUT2}$ → VMH circuit, we delivered AAV9-CaMKIIa-ChR2 (H134R)-GFP into the vSub of wild-type mice (Addgene, #26969, titer: 5×10^{12} GC/ml, 0.2 µl/injection). 4 weeks later, the brain sections containing VMH were subjected to electrophysiological recording. To activate the vSub → VMH pathway, we injected retrograde AAV-Cre into the VMH and delivered AAV9-DIO-ChR2-EYFP (Addgene, #20298, titer: 5×10^{12} GC/ml, 0.2 µl) into the vSub. During the same surgery, an optic fiber (200 µm core, R-FOC-BL200C-39NA, RWD) was placed over the VMH (AP: −1.7 mm; ML: 0.5 mm; DV: −5.4 mm). To inhibit the vSub → VMH pathway, we bilaterally injected retrograde AAV-Cre into the VMH and delivered AAV9-DIO-Arch-GFP (Addgene, #22222, titer: 5×10^{12} GC/ml, 0.2 µl) into the bilateral vSub. During the same surgery, two optic fibers (200 µm core, R-FOC-BL200C-39NA, RWD) were placed over both sides of the vSub (AP: −3.8 mm; ML: ± 3 mm; DV: −4.4 mm).

To simultaneously activate VMH-projecting vSub neurons and inhibition of vSub-innervated neurons in the VMH, LS, or NAcSh, we injected retrograde AAV-Cre into the VMH and delivered Cre-dependent AAV vector carrying ChR2-EYFP (Addgene, #20298-AAV9) into the vSub. During the same surgery, we bilaterally injected an anterograde trans-synaptic AAV1 vector carrying Flpo (Addgene, #55637-AAV1) into the vSub, and bilaterally inject Flpo-dependent AAV harboring hM4Di-mCherry (plasmid was kindly provided by Dr. Huxing Cui and Dr. Deniz Atasoy, virus was packaged by the Baylor IDDRC Neuroconnectivity Core, titer: 1×10^{11} GC/ml, 0.2 µl/injection) into the VMH, LS (AP: 0.7 mm; ML: ±0.3 mm; DV: −3.5 mm), or NAcSh (AP: 0.9 mm; ML: ±0.5 mm; DV: −4.5 mm) in different groups of mice, respectively. An optic fiber (200 µm core, R-FOC-BL200C-39NA, RWD) was placed over the vSub; fibers were fixed to the skull using dental acrylic. To activate VMH-projecting vSub neurons to induce *Fos* expression in the VMH, we bilaterally injected retrograde AAV-Cre into the VMH and AAV-hSyn-DIO-hM3Dq-mCherry (#44361-AAV8, Addgene, 1×10^{11} GC/ml, 0.2 µl/injection) into the vSub.

For di-synaptic tracing of the OB/vSub/VMH pathway, 0.4 µL retrograde AAV-Cre virus was delivered into the VMH, and the helper virus AAV8-FLEX-GTB (Salk, #26197-AAV8, titer: 2.12×10^{11} GC/ml, 0.3 µl/injection) was injected into the vSub of wild-type mice. 21 days later, EnvA-ΔG-Rabies-GFP (Salk, #32635, titer: 6×10^{8} GC/ml, 0.3 µl/injection) was injected into the vSub. Following incubation for 7 days, mice were perfused, and the GFP expression was checked throughout the whole brain.

To inhibit vSub-projecting OB neurons, we bilaterally injected retrograde AAV-Cre into the vSub and injected AAV-EF1a-DIO-Kir2.1-P2A-tdTOMATO (Addgene, #60661, 3.46×10^{11} GC/ml, 0.2 µl/injection) into the OB (AP: 3.6 mm; ML: ±0.9 mm; DV: −1.7 mm). To constant activate the vSub-projecting OB neurons, we bilaterally injected retrograde AAV-Cre into the vSub and injected AAV-EF1a-Flex-EGFP-P2A-mNaChBac (Plasmid was kindly provided by Dr. Benjamin Arenkiel, virus was packaged by the Baylor IDDRC Neuroconnectivity Core, 3.24×10^{12} GC/ml, 0.2 µl/injection) into the OB.

RNAscope

We injected retrograde AAV-Cre (Addgene, #105553-AAVrg, titer: 5×10^{12} GC/ml, 0.2 µl/injection) into the VMH, and a Cre-dependent mCherry virus (AAV8-DIO-mCherry, Addgene, #50459, titer: 5×10^{12} GC/ml, 0.2 µl/injection) into the vSub to label VMH-projecting vSub neurons. Four weeks later, mice were anesthetized and perfused transcardially with 0.9% saline, followed by 10% formalin. Brains were removed and post-fixed in 10% formalin for 16 h at 4 °C and cryoprotected in 30% sucrose for 48 h. Brains were frozen, sectioned at 14 µm using the cryostat, and washed in DEPC-treated phosphate-buffered saline for 10 min. Sections were mounted on DEPC-treated charged slides, dried for 0.5 h at room temperature, and stored at −80 °C. On the day of the RNAScope assay, the slides were thawed, and slides were rinsed 2 times in PBS 1X and placed in an oven for 30 min at 60 °C. After that, slides were post-fixed in 10% formalin for 15 min at 4 °C. Slides were then gradually dehydrated in ethanol (50, 70, and 100%, 5 min each) and underwent target retrieval for 5 min at 100 °C. Slides were incubated in protease III (#322337, ACDBio) for 30 min at 40 °C. Slides were then rinsed in distilled water and incubated in RNAScope probes for *mCherry* (#513201, ACDBio), *Vglut2* (#319171-C3, ACDBio), and *Vgat* (#319191-C2, ACDBio) for 2 h at 40 °C. Sections were then processed using the RNAscope Fluorescent Multiplex Detection Reagents (#320851, ACDBio) according to the manufacturer's instructions. Slides were cover-slipped and analyzed using a fluorescence microscope. Similarly, to determine the molecular identity of excited VMH neurons induced by vSub activation, we injected retrograde AAV-Cre into the VMH and Cre-dependent hM3Dq into the vSub. Four weeks later, mice were administered CNO (3 mg/kg, #16882, Cayman) 45 min prior to perfusion. Following fixation and sectioning, triple RNAscope for *Fos* (#584741-C3, ACDBio), *Vglut2* (#319171, ACDBio), and *Vgat* (#319191-C2, ACDBio) was performed as described above.

Immunohistochemistry

For FO-induced c-Fos immunostaining, WT mice were exposed to odors from 5:30 pm to 6:30 pm to capture peak c-Fos expression following FO exposure. After the odor exposure, mice were anesthetized with inhaled isoflurane and quickly perfused with saline, followed by 10% formalin. The brain sections were cut at 25 μm and collected into five consecutive series. The brain sections containing the vSub were pretreated with 0.3% H_2O_2 for 30 min, then blocked (3% Normal goat serum) for 1 h, incubated with mouse anti-c-Fos antibody (1:2,000; ab208942, Abcam) on shaker at room temperature for overnight, followed by biotinylated goat anti-mouse secondary antibody (1:1,000; BA-9200, Vector) for 2 h. Sections were then incubated in the avidin-biotin complex (1:500, ABC; PK-6101, Vector) and incubated in 0.04% 3,3′-diaminobenzidine and 0.01% hydrogen peroxide. Slides were cover-slipped and imaged using a bright-field microscope. The numbers of c-Fos positive cells in the vSub were counted in 5 consecutive brain sections, and the average was used to reflect the data value for each mouse. Three mice were included in each group for statistical analyses.

Fiber photometry

Mice receiving GCaMP6m injection into vSub rested for 4 weeks to allow for adequate recovery and GCaMP6m expression. Then, mice were habituated for investigator handling and the context of testing box for 1 week before experiment. Mice were fasted for 24 h before the recordings. During the recordings, mice were allowed to freely move in a non-transparent acrylic box (40 cm L × 30 cm W × 40 cm H) with 5 cm deep of clean bedding. In the first experimental paradigm (Fig. 2i), a small amount of bedding (~1 g) carrying either chow-derived odor, isoamyl acetate (ISO), or acetic acid with the same appearance as the clean bedding was put in a random spot of the bedding. In the second experimental paradigm (Supplementary Fig. 4b), mice were allowed to freely move in the same box with 4-odor choice by putting four cell culture dishes (6 cm) with same appearance covered by white filter paper containing chow pellet, HFD pellet, isoamyl acetate (0.5 ml) or acetic acid (0.5) at four corners of the box. A camera was put on the top of the box to monitor the sniffing behavior in recorded mice. Sniffing events were manually annotated and defined as close head orientation and nose towards the odor-containing bedding patch. Only clear sniffing bouts (≥1 s) were used for Ca^{2+} signal alignment. Calcium signals were aligned to the onset of each annotated sniffing event. Continuous <20 μW blue LED at 465 nm and UV LED at 405 nm served as excitation light sources, driven by a multichannel hub (Doric Lenses), modulated at 211 Hz and 330 Hz, respectively. The digital signals were then amplified, demodulated, and collected through a lock-in amplifier (RZ5P, Tucker-Davis Technologies). The fiber photometry data were collected using Synapse 2.0 (Tucker-Davis Technologies) and down-sampled to 8 Hz. For the long-time recordings, mice were habituated in the experimental paradigm used for OE and feeding test (Supplementary Fig. 1c) for 1 week. During the recordings, baseline was recorded for 10 min without 1 kg chow in the bottom container. After baseline recordings, bottom container was changed to one filled with 1 kg chow diet to record another 30 min. Calcium signals were recorded using a dual-color fiber photometry system (Inper Co., Ltd). GCaMP6s was excited by 470 nm channel to record changes of calcium activity, and 410 nm channel as control to exclude disturbances of fluorescent signals caused by artificial factors. The laser power at the tip of the optical fiber was adjusted to be 30 μW for 470 nm excitation channel and 15 μW for the control channel (410 nm) to decrease laser bleaching of fluorescent signals. Averaged traces of Ca^{2+} fluorescent signal changes, area under the curve (AUC) were analyzed and plotted using Inper Plot (V1.7.9) provided by Inper automatically.

Real-time place avoidance test

Real-time place avoidance tests were performed as previously described[66]. Briefly, the same mice used in the excitatory optogenetic studies were used here. All tests were performed in a dedicated soundproof behavioral facility. These mice were brought to the procedure room 1 h before the start of each test and remained in the same room throughout the test. The conditioned place preference apparatus contained two identical conditioning chambers (chambers 1 and 2) that were connected by an opening (10 cm) in the center. Each chamber was 30 × 30 × 30 cm (length × width × height) with white plexiglass walls and floor. Before testing, mice were allowed to explore the two chambers for half an hour during the light cycle. Then, blue light (473 nm, 5 ms/pulse, 20 Hz) was shed when it entered chamber labeled with light on and ceased when it entered chamber labeled with light off indicated in the figure. Time spent in each chamber was recorded and analyzed for chamber preference by experimenters who were blind to experimental information. At end of these experiments, all mice were perfused with 10% formalin. Brain sections were collected, and expression of EYFP and the track were checked. Only those with accurate targeting were included for data analyses.

Slice electrophysiology

Electrophysiology recordings were performed as previously described[67]. Briefly, mice were anesthetized with isoflurane and brains were dissected rapidly and immersed in ice-cold and oxygenated cutting solutions (10 mm NaCl, 195 mm sucrose, 2.5 mm KCl, 1.25 mm NaH_2PO_4, 7 mm $MgCl_2$, 25 mm $NaHCO_3$, 5 mm glucose, 0.5 mm $CaCl_2$, and 2 mm sodium pyruvate, balanced with 95% O_2/5% CO_2). Coronal brain slices (220 μm) containing the targeted region were cut with a Microm HM 650 V vibratome (Thermo Scientific) in oxygenated cutting solution. Slices were then incubated in oxygenated artificial CSF (ACSF; 126 mm NaCl, 2.5 mm KCl, 2.4 mm $CaCl_2$, 1.2 mm NaH_2PO_4, 1.2 mm $MgCl_2$, 11.1 mm glucose, and 21.4 mm $NaHCO_3$, balanced with 95% O_2/5% CO_2, pH 7.4) to recover ~25 min at 32 °C and subsequently for ≧1 h at room temperature before recording.

Slices were then transferred to the recording chamber perfused continuously with 32 °C artificial cerebrospinal fluid bubbled with 95% O_2/5% CO_2 to ensure adequate oxygenation of slices. tdTOMATO (+) neurons were identified by using epifluorescence and IR-DIC imaging on an upright microscope (Eclipse FN-1, Nikon) equipped with a movable stage (MP-285, Sutter Instrument). Patch pipettes with resistances of 3–5 MΩ were filled with intracellular solution (adjusted to pH 7.3) containing 128 mmol/l K gluconate, 10 mmol/l KCl, 10 mmol/l HEPES, 0.1 mmol/l EGTA, 2 mmol/l $MgCl_2$, 0.3 mmol/l Na-GTP, and 3 mmol/l Mg-ATP. Recordings were made using a MultiClamp 700B amplifier (Axon Instrument), sampled using Digidata 1440A, and analyzed offline with pClamp 10.3 software (Axon Instrument). Series resistance was monitored during the recording, and the values were generally <10 MΩ and were not compensated. The liquid junction potential was +12.5 mV and was corrected after the experiment. Data were excluded if the series resistance increased >20% during the experiment or without overshoot for action potential. Currents were amplified, filtered at 1 kHz, and digitized at 20 kHz. Current clamp was engaged to test neural firing frequency at the baseline or in response to light stimulation. For the light-evoked postsynaptic current recordings, the internal recording solution contained: 125 mM $CsCH_3SO_3$; 10 mM CsCl; 5 mM NaCl; 2 mM $MgCl_2$; 1 mM EGTA; 10 mM HEPES; 5 mM (Mg)ATP; 0.3 mM (Na)GTP (pH 7.3 with CsOH). The light-evoked postsynaptic currents were measured in the voltage clamp mode with a holding potential of −70 mV 4-AP and TTX were used to confirm that the light-evoked postsynaptic currents are monosynaptic currents. DNQX (20 μM; an AMPA receptor antagonist) was used to examine whether the postsynaptic currents are excitatory currents.

Statistics

The minimal sample size was predetermined by the nature of experiments. The data are presented as mean ± SEM and/or individual data points. Statistical analyses were performed using GraphPad Prism to

evaluate normal distribution and variations within and among groups. Methods of statistical analyses were chosen based on the design of each experiment and are indicated in figure legends; $P < 0.05$ was considered to be statistically significant.

Reporting summary

Further information on research design is available in the Nature Portfolio Reporting Summary linked to this article.

Data availability

All data supporting the findings of this study are available within the article and its supplementary information files. Source data are provided with this paper.

References

1. Elmaleh-Sachs, A. et al. Obesity management in adults: a review. *JAMA* **330**, 2000–2015 (2023).
2. Dall, T., Sapra, T., Natale, Z., Livingston, T. & Chen, F. Assessing the Economic Impact of Obesity and Overweight on Employers: Identifying Paths Toward Work Force Health and Well-Being. *Nutr. Diabetes* **14**, 96 (2024).
3. Bruning, J. C. & Fenselau, H. Integrative neurocircuits that control metabolism and food intake. *Science* **381**, eabl7398 (2023).
4. Gao, Q. & Horvath, T. L. Neuronal control of energy homeostasis. *FEBS Lett.* **582**, 132–141 (2008).
5. Waterson, M. J. & Horvath, T. L. Neuronal regulation of energy homeostasis: beyond the hypothalamus and feeding. *Cell Metab.* **22**, 962–970 (2015).
6. Jovanovic, P. & Riera, C. E. Olfactory system and energy metabolism: a two-way street. *Trends Endocrinol. Metab.* **33**, 281–291 (2022).
7. Boesveldt, S. & de Graaf, K. The differential role of smell and taste for eating behavior. *Perception* **46**, 307–319 (2017).
8. Soria-Gomez, E., Bellocchio, L. & Marsicano, G. New insights on food intake control by olfactory processes: the emerging role of the endocannabinoid system. *Mol. Cell. Endocrinol.* **397**, 59–66 (2014).
9. Yeomans, M. R. J. P. & behavior. Olfactory influences on appetite and satiety in humans. *Physiol. Behav.* **87**, 800–804 (2006).
10. Morquecho-Campos, P., de Graaf, K. & Boesveldt, S. J. F. Q. & Preference. Smelling our appetite? The influence of food odors on congruent appetite, food preferences and intake. *Food Qual. Prefer.* **85**, 103959 (2020).
11. Horio, N. & Liberles, S. D. Hunger enhances food-odour attraction through a neuropeptide Y spotlight. *Nature* **592**, 262–266 (2021).
12. Jansen, A. et al. Overweight children overeat after exposure to food cues. *Eat. Behav.* **4**, 197–209 (2003).
13. Lushchak, O. V., Carlsson, M. A. & Nassel, D. R. Food odors trigger an endocrine response that affects food ingestion and metabolism. *Cell. Mol. Life Sci.* **72**, 3143–3155 (2015).
14. Massolt, E. T. et al. Appetite suppression through smelling of dark chocolate correlates with changes in ghrelin in young women. *Regul. Pept.* **161**, 81–86 (2010).
15. Witter, M. P. & Groenewegen, H. J. The subiculum: cytoarchitectonically a simple structure, but hodologically complex. *Prog. Brain Res.* **83**, 47–58 (1990).
16. Tang, H. et al. Brain-wide map of projections from mice ventral subiculum. *Neurosci. Lett.* **629**, 171–179 (2016).
17. Wee, R. W. S. & MacAskill, A. F. Biased connectivity of brain-wide inputs to ventral subiculum output neurons. *Cell Rep.* **30**, 3644–3654.e3646 (2020).
18. Herman, J. P. & Mueller, N. K. Role of the ventral subiculum in stress integration. *Behav. Brain Res.* **174**, 215–224 (2006).
19. Herman, J. P., Dolgas, C. M. & Carlson, S. L. Ventral subiculum regulates hypothalamo-pituitary-adrenocortical and behavioural responses to cognitive stressors. *Neuroscience* **86**, 449–459 (1998).
20. Yan, J. J. et al. A circuit from the ventral subiculum to anterior hypothalamic nucleus GABAergic neurons essential for anxiety-like behavioral avoidance. *Nat. Commun.* **13**, 7464 (2022).
21. O'Mara, S. M., Sanchez-Vives, M. V., Brotons-Mas, J. R. & O'Hare, E. Roles for the subiculum in spatial information processing, memory, motivation and the temporal control of behaviour. *Prog. Neuropsychopharmacol. Biol. Psychiatry* **33**, 782–790 (2009).
22. Marchant, N. J. et al. Role of ventral subiculum in context-induced relapse to alcohol seeking after punishment-imposed abstinence. *J. Neurosci.* **36**, 3281–3294 (2016).
23. Wikenheiser, A. M., Marrero-Garcia, Y. & Schoenbaum, G. Suppression of Ventral Hippocampal Output Impairs Integrated Orbitofrontal Encoding of Task Structure. *Neuron* **95**, 1197–1207.e1193 (2017).
24. Cooper, D. C., Klipec, W. D., Fowler, M. A. & Ozkan, E. D. A role for the subiculum in the brain motivation/reward circuitry. *Behav. Brain Res.* **174**, 225–231 (2006).
25. Burhans, L. B. & Gabriel, M. Contextual modulation of conditioned responses: role of the ventral subiculum and nucleus accumbens. *Behav. Neurosci.* **121**, 1243–1257 (2007).
26. Petrulis, A., Alvarez, P. & Eichenbaum, H. Neural correlates of social odor recognition and the representation of individual distinctive social odors within entorhinal cortex and ventral subiculum. *Neuroscience* **130**, 259–274 (2005).
27. Mohammad, H. et al. A neural circuit for excessive feeding driven by environmental context in mice. *Nat. Neurosci.* **24**, 1132–1141 (2021).
28. Kim, K. W. et al. Steroidogenic factor 1 directs programs regulating diet-induced thermogenesis and leptin action in the ventral medial hypothalamic nucleus. *Proc. Natl. Acad. Sci. USA* **108**, 10673–10678 (2011).
29. Kim, K. W. et al. SF-1 in the ventral medial hypothalamic nucleus: a key regulator of homeostasis. *Mol. Cell. Endocrinol.* **336**, 219–223 (2011).
30. Dhillon, H. et al. Leptin directly activates SF1 neurons in the VMH, and this action by leptin is required for normal body-weight homeostasis. *Neuron* **49**, 191–203 (2006).
31. Viskaitis, P. et al. Modulation of SF1 neuron activity coordinately regulates both feeding behavior and associated emotional states. *Cell Rep.* **21**, 3559–3572 (2017).
32. Fujikawa, T. et al. SF-1 expression in the hypothalamus is required for beneficial metabolic effects of exercise. *eLife* **5**, e18206 (2016).
33. Musatov, S. et al. Silencing of estrogen receptor alpha in the ventromedial nucleus of hypothalamus leads to metabolic syndrome. *Proc. Natl. Acad. Sci. USA* **104**, 2501–2506 (2007).
34. Correa, S. M. et al. An estrogen-responsive module in the ventromedial hypothalamus selectively drives sex-specific activity in females. *Cell Rep.* **10**, 62–74 (2015).
35. de Morentin, P. B. M. et al. Estradiol regulates brown adipose tissue thermogenesis via hypothalamic AMPK. *Cell Metab.* **20**, 41–53 (2014).
36. Zhang, J., Chen, D., Sweeney, P. & Yang, Y. J. N. c. An excitatory ventromedial hypothalamus to paraventricular thalamus circuit that suppresses food intake. *Nat. Commun.* **11**, 1–14 (2020).
37. Coutinho, E. A. et al. Activation of SF1 neurons in the ventromedial hypothalamus by DREADD technology increases insulin sensitivity in peripheral tissues. *Diabetes* **66**, 2372–2386 (2017).
38. King, B. M., Carpenter, R. G., Stamoutsos, B. A., Frohman, L. A. & Grossman, S. P. Hyperphagia and obesity following ventromedial hypothalamic lesions in rats with subdiaphragmatic vagotomy. *Physiol. Behav.* **20**, 643–651 (1978).
39. Carvalho, V. M. A. et al. Representation of olfactory information in organized active neural ensembles in the hypothalamus. *Cell Rep.* **32**, 108061 (2020).

40. Rao, B. S. & Prabhakar, E. Effects of body weight loss and taste on VMH-LH electrical activity of rats. *Physiol. Behav.* **52**, 1187–1192 (1992).
41. Lanuza, E. et al. Sex pheromones are not always attractive: changes induced by learning and illness in mice. *Anim. Behav.* **97**, 265–272 (2014).
42. Fallon, N., Giesbrecht, T. & Stancak, A. Attentional modulation of desensitization to odor. *Atten. Percept. Psychophys.* **80**, 1064–1071 (2018).
43. McBride, K., Slotnick, B. & Margolis, F. L. Does intranasal application of zinc sulfate produce anosmia in the mouse? An olfactometric and anatomical study. *Chem. Senses* **28**, 659–670 (2003).
44. Adilbay, D. et al. Noninvasive diagnostic method to objectively measure olfaction and diagnose smell disorders by a molecularly targeted fluorescence imaging agent. *J. Nucl. Med.* **65**, 1293–1300 (2024).
45. Bekkers, J. M. & Suzuki, N. Neurons and circuits for odor processing in the piriform cortex. *Trends Neurosci.* **36**, 429–438 (2013).
46. Fu, L. Y. & van den Pol, A. N. Agouti-related peptide and MC3/4 receptor agonists both inhibit excitatory hypothalamic ventromedial nucleus neurons. *J. Neurosci.* **28**, 5433–5449 (2008).
47. Ulrich-Lai, Y. M., Fulton, S., Wilson, M., Petrovich, G. & Rinaman, L. Stress exposure, food intake and emotional state. *Stress* **18**, 381–399 (2015).
48. Sweeney, P. & Yang, Y. An inhibitory septum to lateral hypothalamus circuit that suppresses feeding. *J. Neurosci.* **36**, 11185–11195 (2016).
49. Stratford, T. R. & Kelley, A. E. GABA in the nucleus accumbens shell participates in the central regulation of feeding behavior. *J. Neurosci.* **17**, 4434–4440 (1997).
50. Zhu, C. et al. Profound and redundant functions of arcuate neurons in obesity development. *Nat. Metab.* **2**, 763–774 (2020).
51. Lane, G., Zhou, G., Noto, T. & Zelano, C. Assessment of direct knowledge of the human olfactory system. *Exp. Neurol.* **329**, 113304 (2020).
52. Boone, M. H., Liang-Guallpa, J. & Krashes, M. J. Examining the role of olfaction in dietary choice. *Cell Rep.* **34**, 108755 (2021).
53. Riera, C. E. et al. The sense of smell impacts metabolic health and obesity. *Cell Metab.* **26**, 198–211 e195 (2017).
54. Miro, J., Canguilhem, B., Schmitt, P. & Koch, A. J. P. & behavior. Hyperphagia and obesity after olfactory bulbectomy performed at different times of the year in the European hamster. *Physiol. Behav.* **29**, 681–685 (1982).
55. Primeaux, S. D., Barnes, M. J. & Bray, G. A. J. B. b. r. Olfactory bulbectomy increases food intake and hypothalamic neuropeptide Y in obesity-prone but not obesity-resistant rats. *Behav. Brain Res.* **180**, 190–196 (2007).
56. Keller, A. & Malaspina, D. Hidden consequences of olfactory dysfunction: a patient report series. *BMC Ear Nose Throat Disord.* **13**, 8 (2013).
57. Fadool, D. A. et al. Kv1.3 channel gene-targeted deletion produces "Super-Smeller Mice" with altered glomeruli, interacting scaffolding proteins, and biophysics. *Neuron* **41**, 389–404 (2004).
58. Tucker, K., Overton, J. M. & Fadool, D. A. Diet-induced obesity resistance of Kv1.3-/- mice is olfactory bulb dependent. *J. Neuroendocrinol.* **24**, 1087–1095 (2012).
59. Fanselow, M. S. & Dong, H. W. Are the dorsal and ventral hippocampus functionally distinct structures?. *Neuron* **65**, 7–19 (2010).
60. Ding, S. L. et al. Distinct transcriptomic cell types and neural circuits of the subiculum and prosubiculum along the dorsal-ventral axis. *Cell Rep.* **31**, 107648 (2020).
61. Singh, U. et al. Collateralizing ventral subiculum melanocortin 4 receptor circuits regulate energy balance and food motivation. *Physiol. Behav.* **262**, 114105 (2023).
62. Kosse, C., Ivanov, J., Knight, Z., Pellegrino, K. & Friedman, J. A subcortical feeding circuit linking an interoceptive node to jaw movement. *Nature* **636**, 151–161 (2024).
63. Sweeney, P. & Yang, Y. Neural circuit mechanisms underlying emotional regulation of homeostatic feeding. *Trends Endocrinol. Metab.* **28**, 437–448 (2017).
64. Wee, R. W. S. et al. Internal-state-dependent control of feeding behavior via hippocampal ghrelin signaling. *Neuron* **112**, 288–305.e287 (2024).
65. Bergman, U., Ostergren, A., Gustafson, A. L. & Brittebo, B. Differential effects of olfactory toxicants on olfactory regeneration. *Arch. Toxicol.* **76**, 104–112 (2002).
66. Cai, J. et al. An excitatory projection from the basal forebrain to the ventral tegmental area that underlies anorexia-like phenotypes. *Neuron* **112**, 458–472.e456 (2024).
67. Liu, H. et al. A light-responsive neural circuit suppresses feeding. *J. Neurosci.*https://doi.org/10.1523/JNEUROSCI.2192-23.2024 (2024).

Acknowledgements

The investigators were supported by grants from Texas Children's Research Scholar funds to Y.H.; American Heart Association (23POST1030352 to H.-L.L.), the USDA/CRIS (51000-064-01S to Y.X., 3092-51000-062-04(B)S to C.W.), NIH (R01DK140538 to Y.H., R01DK138518 and R01DK138123 to Y.X., DK136284, R01 DK 135212 and R01 DK 131466 to Q.-C.T.), CPRIT Scholar in Cancer Research (RR200063), NIH/NIA U01 AG086143, the Longevity Impetus Grant, Ted Nash Long Life Foundation, and the Welch Foundation to H.-J.L. We also thank Dr. Ariel Lyons-Warren and Dr. Hugo J. Bellen for their intellectual contributions to the manuscript.

Author contributions

Y.H. and Y.X. designed the study, supervised the work, and wrote the manuscript. Y.L. and H.-L.L. performed most of the experiments, data acquisition, and analysis. Y.H. conducted electrophysiological recordings and data analysis. N.A. assisted in the acute feeding experiments. H.-X.K.W., K.M.C., Y.X.L., M.Y., Y.D., Q.L., X.F., M.W., Y.S., O.Z.G., Y.X.Y., L.T., H.S.L., J.C.B., J.H., M.E.B., S.V.J., and Y.J.Y. contributed to the generation of study mice. H.-J.L., C.W., Q.-C.T., and B.R.A. were involved in data discussion and contributed intellectually to the manuscript.

Competing interests

The authors declare no competing interests.

Ethical approval

Care of all animals and procedures was approved by the Baylor College of Medicine Institutional Animal Care and Use Committee.

Additional information

Supplementary information The online version contains supplementary material available at https://doi.org/10.1038/s41467-025-63170-2.

Correspondence and requests for materials should be addressed to Yong Xu or Yang He.

Peer review information *Nature Communications* thanks the anonymous reviewers for their contribution to the peer review of this work. A peer review file is available.